IEEE Access
Multidisciplinary | Rapid Review | Open Access Journal

Received May 20, 2020, accepted May 29, 2020, date of publication June 5, 2020, date of current version July 2, 2020.

Digital Object Identifier 10.1109/ACCESS.2020.3000462

Neuro Fuzzy Logic Controlled Parallel Resonance Type Fault Current Limiter to Improve the Fault Ride Through Capability of DFIG Based Wind Farm

MD. RASHIDUL ISLAM[1], JAKIR HASAN[1], MD. REZAUR RAHMAN SHIPON[1], MOHAMMAD ASHRAF HOSSAIN SADI[2], (Senior Member, IEEE), AHMED ABUHUSSEIN[3], (Member, IEEE), AND TUSHAR KANTI ROY[4]

[1]Department of Electrical and Electronic Engineering, Rajshahi University of Engineering and Technology, Rajshahi 6204, Bangladesh
[2]College of Health, Science, and Technology, University of Central Missouri, Warrensburg, MO 64093, USA
[3]Department of Electrical and Computer Engineering, Gannon University, Erie, PA 16541, USA
[4]Department of Electronics and Telecommunication Engineering, Rajshahi University of Engineering and Technology, Rajshahi 6204, Bangladesh

Corresponding author: Md. Rashidul Islam (rashidul@eee.ruet.ac.bd)

ABSTRACT Doubly fed induction generators (DFIGs) are vulnerable to grid related electrical faults. Standards require DFIGs to be disconnected from the grid unless augmented with a fault ride through (FRT) capability. A fault current limiter (FCL) can enhance the overall stability of wind farms and allow them to maintain grid-code requirements. In this paper, a neuro fuzzy logic controlled parallel resonance type fault current limiter (NFLC-PRFCL) is proposed to enhance the FRT capability of the DFIG based wind farm. Theoretical and graphical analysis of the proposed method are carried out by MATLAB/Simulink software. The performance of the NFLC-PRFCL is compared with other documented FCL devices, e.g., the bridge type fault current limiter (BFCL) and the series dynamic braking resistor (SDBR). The performance of the NFLC-PRFCL is also compared with that of the existing fuzzy logic controlled parallel resonance fault current limiter (FLC-PRFCL). From the simulation results, it is found that the NFLC-PRFCL outperforms its competitors and enables the DFIG to maintain a near-seamless performance during various fault events.

INDEX TERMS Doubly fed induction generator (DFIG), fault ride through (FRT), fuzzy logic controller (FLC), neuro fuzzy logic controller (NFLC), parallel resonance fault current limiter (PRFCL).

I. INTRODUCTION

Due to the depletion of traditional fossil fuels and global rising of environmental issues, the use of alternative renewable energy sources (RESs) such as solar photovoltaic (PV) units, wind power generators, geothermal power, hydro power, fuel cells, etc. are getting more attention to meet the increasing power demand. However, among these RESs, the solar PV units and wind power generators are the most promising alternative energy sources due to their unique properties [1], [2]. But, due to the technological developments, currently, the wind power generator is one of the fastest rising RESs for the generation of electrical energy. Nowadays, the doubly fed induction generator (DFIG) based wind farm has got more attention owing to the properties of controllable output power, low cost of installation etc. as compared to a squirrel cage induction generator (SCIG) based wind farm. However, the DFIG based wind farms are very sensitive to utility grid disturbances, especially to voltage sag during grid faults [3]. Hence, fault ride through (FRT) capability of a grid-connected DFIG based wind farm is required in order to maintain the grid codes which are referred by power system operators all around the world [4], [5].

The FRT capability enhancement of a grid-connected DFIG based wind farm is a prime concern to augment the transient stability since the stability of the entire utility grid depends on it [6], [7]. During a fault, a DFIG based wind farm should remain connected to the grid without exceeding certain voltage and frequency limits. The grid codes of different countries are shown in Fig. 1. The grid code of the United States (FERC) is followed and maintained throughout this work. According to this grid code, to stay online with the

The associate editor coordinating the review of this manuscript and approving it for publication was Seyyed Ali Pourmousavi Kani.

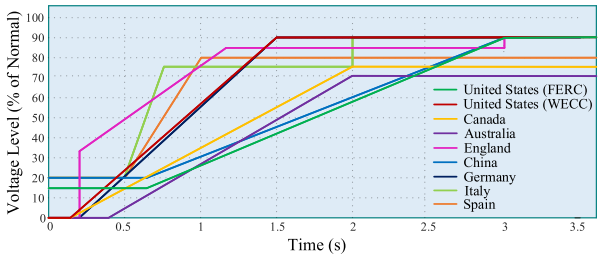

FIGURE 1. Grid codes of different countries.

grid, the maximum permissible voltage dip is up to 15% of the nominal value in a time span of 0.625s. Then the voltage must restore to 90% of the nominal value within 3s.

So far in the literature, several strategies have been adopted for DFIG based wind farms to augment their FRT capability. The solutions can be mainly categorized into three different types i.e., hardware implementation, controller development for DFIG converters, and a cooperation of the hardware implementation and software control strategy development [8]. The software solutions incorporate strategies like demagnetizing control [9], [10], inductance emulating control (IEC) [8], [11], and flux linkage tracking control (FLTC) [12]. But the software control strategies are only useful for suppressing the rotor over-current under moderate voltage sags. Although the IEC can deal with up to 80% voltage sags, protection against 100% voltage sags is not feasible with software control. Moreover, the software control strategy cannot suppress the high peak value of rotor current during transmission line fault and thus no reactive power control is possible [8]. Hence the reactive power supplied by the DFIG during faults is inadequate to support the PCC during system faults.

Implementing hardware solutions can solve the problems with software control strategy by improving the DFIG terminal voltage significantly. Hardware solutions can incorporate crowbars [13], flexible AC transmission system (FACTS) devices [14], [15], energy storage systems [16], [17], DC choppers [18] etc. But the hardware solutions demand additional converters and transformers, thus increasing the total cost of installation and maintenance. They are also complex in topology and unreliable for small wind turbine system. Compromising the limitations of the hardware solutions and software control strategies, a cooperative control approach was developed. Several cooperative control schemes have been developed in literature over the years [19], [20]. The hardware part of these schemes take care of the DFIG terminal voltage and the software part suppress the rotor over-current and electromagnetic torque oscillations.

The solutions discussed so far are useful for new installations only. Thus, the flexibility of these control schemes is limited. However, the hardware solutions that incorporates auxiliary devices are flexible and cost effective for both new and old installations. To improve the FRT capability of DFIG based wind farms, use of auxiliary devices like fault current limiters (FCLs) are proven to be useful in minimizing the fault current and restore the stability of the system [5]. In order to

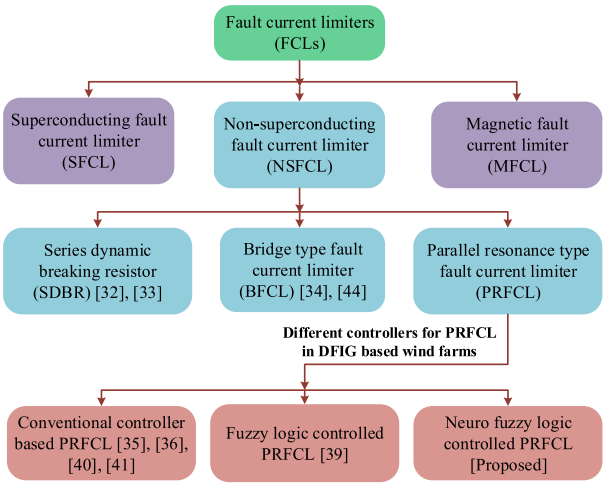

FIGURE 2. Classification of fault current limiters.

improve the FRT capability, several kinds of FCLs are proposed in the literature over the years [21]–[25]. Among them, three types of FCLs namely superconducting FCLs (SFCLs), non-superconducting FCLs (NSFCLs), and magnetic FCLs (MFCLs) are widely used due to their own advantages to improve the FRT during grid faults. The classification of the FCLs is shown in Fig. 2. The SFCLs are one of the most popular FCLs to improve the FRT capability in a power system as they are excellent to minimize the fault current [23]. But its application is fairly recent addition in DFIG-based wind farms [26]. In the literature, there are discussions of coordinated applications of the SFCLs with other auxiliary devices too [27]–[30]. But the application of the SFCL is limited due to its complex structure, high implementation cost, and need of liquid cryogenic systems.

On the other hand, the applications of the MFCLs has been discussed in various literature due to their excellent performance to improve the stability of the power system during grid faults [24], [31]. However, the efficiency of the MFCL decreases due to over use of the weaker permanent magnet.

This paper mainly focuses on the use NSFCLs as they have reduced cost while ensuring the same degree of stability [22]. There are several types of NSFCLs as shown in Fig. 2. Series dynamic braking resistors (SDBRs) are one of the most used FCL devices that was proposed in [32], [33], but it has been shown in [34] that, bridge-type fault current limiters (BFCLs) are superior to the SDBRs in terms of enhancing the FRT capability. Parallel resonance type fault current limiter (PRFCL) was proposed in [25] and soon gained popularity as it proved to be superior to the BFCLs in power system applications [35], [36]. The PRFCL augments the transient stability using the principle of resonance condition of a parallel configuration of inductor and capacitor [25], [35], [36]. Being a NSFCL, the PRFCL is cost effective compared to the SFCLs as it uses copper coils instead of costly superconductors [25]. The PRFCL can limit the fault current significantly and in addition to that, it offers an advantage by improving the power quality of distribution system [25].

The effectiveness of cooperative control of hardware solutions with software control strategy is discussed in the previous section. As the power system characteristic is highly nonlinear in nature, any nonlinear controller with FCL would yield better performance instead of using the FCL alone [37], [38]. The controllers which work on the basis of feedback are more effective than the conventional controllers [37]. Feedback controller takes different actions on the basis of fault severity, but in case of conventional controller, some predefined actions are done without measuring the severity and system condition. In the literature, there are fuzzy logic and conventional controllers proposed for controlling the operation of the PRFCL [25], [35], [36], [39]–[41], as represented in Fig. 2. However, the conventional control schemes [35], [36], [40], [41] has some degree of tracking errors as well as steady state errors. Further, their effectiveness depends mainly on the determination of proper reference value. Literature agrees that fuzzy logic as a nonlinear controller [39] performs way better than those conventional controllers. However, the fuzzy logic controller (FLC) depends on some estimated variables and lacks feedback signals [42]. So, there is a gap in the literature for in-depth analysis and feasibility of the dynamic effective nonlinear controller for the PRFCL. On the other hand, the neuro fuzzy logic controller (NFLC) provides the facility to train the FLC on the basis of some real data and assures more effective result [42], [43]. It provides the advantages of both artificial neural network (ANN) and fuzzy logic. In addition, it provides robustness and training in data driven environment [42], [43].

Based on these backgrounds, in this work, a neuro fuzzy logic controlled PRFCL (NFLC-PRFCL) is proposed to augment the FRT capability of DFIG based wind farms. To evaluate the performance of the proposed NFLC-PRFCL, its performance is compared with that of the conventional SDBR [32], [33], BFCL [34], [44] and fuzzy logic controlled PRFCL (FLC-PRFCL) [39].

The rest of the paper is organized as follows: Section II discusses the mathematical modeling of DFIG; Section III discusses the construction of the system model; In section IV, the construction, operating principle and different control techniques of PRFCL are discussed; The construction and working principle of the BFCL and the SDBR are presented in section V; In section VI, the graphical and numerical analysis of different control schemes are carried out for both temporary and permanent faults; Section VII provides an in-depth discussion about the ability of used method in terms of efficiency, effectiveness and accuracy in solving the issues; Section VIII provides a comparative cost analysis of different FRT strategies that we used in this work. Finally, the conclusions are drawn in section IX.

II. MATHEMATICAL MODELING OF DFIG BASED WIND FARMS

In this section, the mathematical modeling of a DFIG based wind turbine will be briefly presented. In order to describe the whole system dynamics, three different types of mathematical models are considered in this work which are discussed in the following subsections.

A. WIND POWER MODELING

The wind turbines are rotary devices which are used to convert the wind energy into electrical energy by driving electrical generators. The magnitude of the extracted power from a wind energy depends on the wind velocity and the air density which can be explained using the following equation [34], [45]–[47]:

$$P_\omega = \frac{1}{2}\pi\rho R^2 V_\omega^3 C_p(\lambda, \beta) \tag{1}$$

where the symbols used in (1) have their usual meanings, which can be found in [37]. However, the performance coefficient is also known as a power coefficient which can be expressed as a function of the blade pitch angle, β and tip speed ratio, λ as follows:

$$C_p(\lambda, \beta) = \frac{1}{2}(\lambda - 0.022\beta^2 - 5.6)e^{-0.17\lambda} \tag{2}$$

The tip speed ratio, λ can be further expressed as:

$$\lambda = \frac{\omega_r R}{V_\omega} \tag{3}$$

where ω_r is the mechanical angular velocity of the wind turbine blade. The electrical mathematical model of a DFIG based wind turbine under both normal and fault conditions is discussed in the following subsections.

B. ELECTRICAL MODELING OF A DFIG UNDER NORMAL CONDITION

For electrical modeling of a DFIG, the commonly and widely used model is the Park's transformation model in which the stator side is considered as a reference frame [48]. It is noted here that the generated reference frame is very useful to analyze the electrical characteristics of a DFIG based wind turbine under both normal and fault conditions. Therefore, to accomplish the aforesaid objective, the stator voltage and rotor voltage of a DFIG can be represented using the following equations [5], [37], [48], [49]:

$$\vec{u_s} = R_s\vec{i_s} + \frac{d}{dt}\vec{\lambda_s} \tag{4}$$

$$\vec{u_r} = R_r\vec{i_r} + \frac{d}{dt}\vec{\lambda_r} - j\omega_m\vec{\lambda_r} \tag{5}$$

where the symbols have their usual meanings, which can be found in [5], [37], [48], [49]. The induced fluxes in the stator and rotor sides of a DFIG can be expressed as follows:

$$\vec{\lambda_s} = L_s\vec{i_s} + L_m\vec{i_r} \tag{6}$$

$$\vec{\lambda_r} = L_r\vec{i_r} + L_m\vec{i_s} \tag{7}$$

where each symbol have their usual meaning, which are defined in [37]. However, the mathematical expression of

leakage inductances (L_s and L_r) can be represented using the following equations:

$$L_s = L_{ls} + L_m \tag{8}$$

$$L_r = L_{lr} + L_m \tag{9}$$

To make it more understandable, an equivalent circuit diagram of a DFIG using equations (8) and (9) is shown in Fig. 3. After performing the mathematical manipulation of (6) and (7), the space vector of the rotor flux can be written as follows:

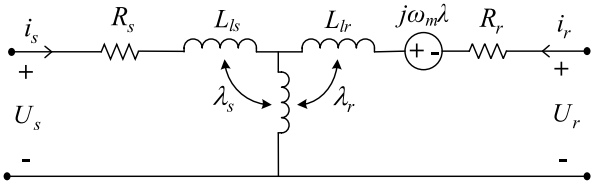

FIGURE 3. Equivalent circuit of DFIG.

$$\vec{\lambda_r} = \frac{L_m}{L_s}\vec{\lambda_s} - \sigma L_r \vec{i_r} \tag{10}$$

where,

$$\sigma = 1 - \frac{L_m^2}{L_s L_m} \tag{11}$$

Using the value of $\vec{\lambda_r}$, (6) can be rewritten as follows:

$$\vec{u_r} = \frac{L_m}{L_s}\left(\frac{d}{dt} - j\omega_m\right)\vec{\lambda_s} + \left(R_r + \sigma L_r\left(\frac{d}{dt} - j\omega_m\right)\right)\vec{i_r} \tag{12}$$

At this stage, in order to obtain the open-circuit rotor voltage, $\vec{u_{r0}}$, we can set $\vec{i_r} = 0$ in (12), which can be written as follows:

$$\vec{u_{r0}} = \frac{L_m}{L_s}\left(\frac{d}{dt} - j\omega_m\right)\vec{\lambda_s} \tag{13}$$

For the sake of simplicity, the value of the transient reactance and the rotor resistance can be neglected and under this condition, the right hand side of (12) is smaller as compared to $\vec{u_{r0}}$. Using this condition, the expression of $\vec{u_{r0}}$ can be rewritten as follows:

$$\vec{u_{r0}} = j\omega_r \frac{L_m}{L_s}\vec{\lambda_s} = \frac{L_m}{L_s}\frac{\omega_r}{\omega_s}U_s e^{j\omega_s t} \tag{14}$$

In (14), ω_r and ω_s are the synchronous and angular frequencies of the slip, respectively. Now, from (14), the magnitude of $\vec{u_{r0}}$ can be written as follows:

$$U_{r0} = \frac{L_m}{L_s}\frac{\omega_r}{\omega_s}U_s = \frac{L_m}{L_s}sU_s \tag{15}$$

where s is the slip which can be expressed as:

$$s = \frac{\omega_s - \omega_m}{\omega_s} \tag{16}$$

Similarly, the slip angular frequency can be expressed as:

$$\omega_r = \omega_s - \omega_m \tag{17}$$

From (15), it can be seen that the rotor voltage of the DFIG has a proportional relation with the slip and the stator voltage. Since, the performance of the proposed method also considers the analysis for a fault condition, it is essential to represent the mathematical model of the DFIG under this condition which is discussed in the following subsection.

C. MATHEMATICAL MODELING OF A DFIG UNDER FAULT CONDITION

It is well-known that, at the instant of a fault, the open-circuit voltage experiences a drastic change in its magnitude. The mathematical representation of an open-circuit voltage under a fault condition can be express as follows [5], [48], [49]:

$$\vec{u_{r0}} = -\frac{L_m}{L_s}\left(j\omega_m + \frac{1}{\tau_s}\right)\frac{U_s}{j\omega_s}e^{j\omega_s t_0}e^{-\frac{t}{\tau_s}} \tag{18}$$

As the direction of this open circuit voltage is opposite to the angular frequency, ω_m, the mathematical representation of this rotating voltage can be expressed using the following equation:

$$\vec{u_{r0}^r} = -\frac{L_m}{L_s}\left(j\omega_m + \frac{1}{\tau_s}\right)\frac{U_s}{j\omega_s}e^{j\omega_s t_0}e^{j\omega_m t}e^{-\frac{t}{\tau_s}} \tag{19}$$

It is obvious that the value of $|\ \vec{u_{r0}^r}\ |$ reaches its peak during the fault period. Since the value of $\frac{1}{\tau_s}$ will be very small as time goes to infinity, the second term in (19) will be negligible as compared to the first term. Based on this condition, (19) can be rewritten as follows:

$$U_{r0}(t_0) = \frac{L_m}{L_s}\frac{\omega_m}{\omega_s}U_s = \frac{L_m}{L_s}(1-s)U_s \tag{20}$$

From (20), it can be seen that during a fault condition, the open circuit rotor voltage is proportional to $(1-s)$. On the other hand, during a normal condition, this open-circuit rotor voltage is proportional to s as seen from (15). The whole system model description along with the control scheme of a DFIG based wind farm is discussed in the following section.

III. SYSTEM MODEL

In this work, detail modeling of the test system including the wind generators and the PRFCL is carried out extensively through a 9 MVA wind farm consisting of six DFIGs rated at 1.5 MVA each as represented in Fig. 4. The wind generator model involves complete power electronic switching circuits, proper adaptive control, and double circuit transmission line. The rotor side converter (RSC) and the grid side converter (GSC) of each DFIG are linked with each other through a DC-link capacitor. The output of each DFIG is stepped up to 66 KV and supplied to the parallel transmission lines. The transmission lines are modeled with impedance and circuit breakers. The simulation design and results are carried out in the MATLAB/Simulink environment. The parameters of each identical DFIG are presented in Appendix. The PRFCL is placed between the point of common coupling (PCC) and the parallel transmission lines.

A. THE RSC AND GSC OF THE DFIG

In this section, the RSC controller and the GSC controller of the DFIG are discussed. The RSC of the DFIG interfaces

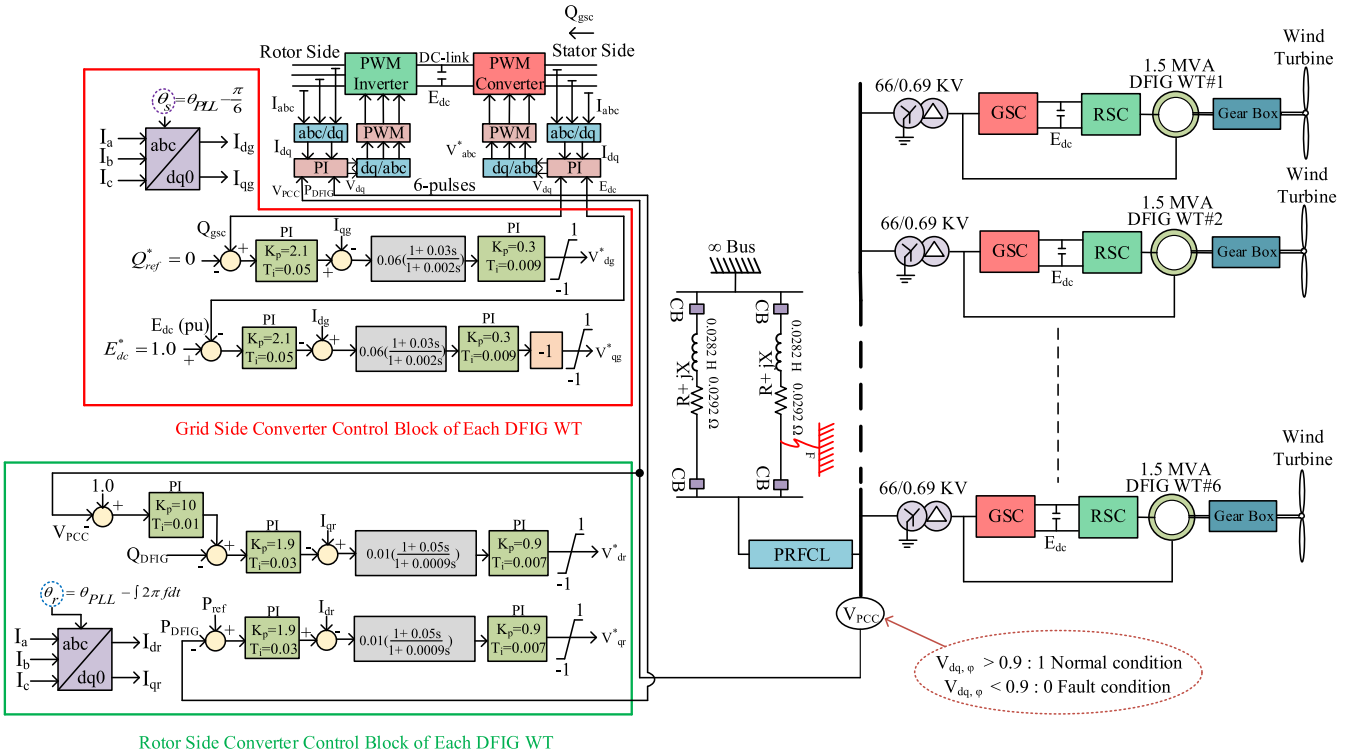

FIGURE 4. Diagram of the study system.

the rotor side with the DC-link capacitor through an insulated gate bipolar transistor (IGBT) based six pulse two level full bridge power converter. The RSC of the DFIG is responsible for controlling the active and reactive power injection at the PCC. In this work, the active and reactive power is controlled using the d-axis and q-axis current in such a way that it regulates the PCC voltage to 1.0 per unit (pu). To achieve such objectives, it is essential to control the gate pulses of the IGBT switch. In this work, a proportional integral (PI) controller is used to get the control signal in the rotating dq-frame. Therefore, the grid abc voltage/current is transformed into dq voltage/current using the Park's transformation. However, before applying the dq-frame control signal to the IGBT switch through a pulse width modulation (PWM) signal generator, it is converted to abc-frame using the inverse Park's transformation as represented in Fig. 4.

The GSC interfaces the grid with the DC side of the DC-link capacitor with IGBT based six pulse two level bridge converter. The GSC is responsible for controlling the DC-link voltage and in this work, the reference voltage of the DC-link capacitor is considered as 1.0 pu. To maintain a stable operation during any fault condition of the system, it is essential to maintain a constant DC-link voltage. Therefore, to achieve such control objectives, similar to the RSC, it is necessary to control gate pulses of the IGBT switch. In this paper, to get the IGBT gate pulses, a PI controller is used to track the reference DC-link voltage which is clearly shown in Fig. 4. In this work, PI controllers' and transfer functions' values of the system model are taken from [47].

IV. PARALLEL RESONANCE TYPE FAULT CURRENT LIMITER (PRFCL)

A. ARCHITECTURE OF THE PRFCL

The architecture of PRFCL is shown in Fig. 5. There are mainly two parts of a PRFCL [25], [35], [36], [39]–[41]:

1) The bridge part: The bridge is formed by four diodes, $D_1 - D_4$. A DC reactor, L_{dc} in series with a IGBT switch is placed inside the diode bridge. The inherent small resistance of the L_{dc} is also considered here by placing a resistor, R_{dc} in series with the L_{dc}. The diode, D_5 is called the free-wheeling diode, used for the safe operation of the L_{dc}.
2) The resonance part: This part consists of an inductor, L_{sh} and a capacitor, C_{sh} connected in parallel. The parallel combination of L_{sh} and C_{sh} forms a resonance circuit. The resonance frequency is the power line frequency. The standard value of C_{sh} is adopted from [50] and considering the resonant condition at power frequency, the value of L_{sh} was calculated. Among all other explored combinations, $C_{sh} = 50\ \mu F$ and $L_{sh} = 141\ mH$ provides the best performance for our work.

B. OPERATING PRINCIPLE OF THE PRFCL

During normal operating condition, the IGBT remains closed and the bridge circuit carries total line current. During positive half cycle, the path connecting D_1, L_{dc}, R_{dc}, D_4 is active and the path connecting D_2, L_{dc}, R_{dc}, D_3 is active during the

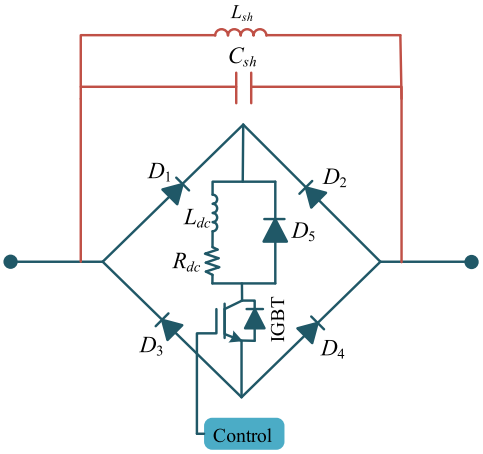

FIGURE 5. Architecture of the PRFCL.

negative half cycle and carries the line current. During both half cycles, the direction of current flowing through the L_{dc} is same. As the current flowing into the L_{dc} is in the same direction, it is charged up to the peak value of the current and smooths out the current ripple. Though some diode forward voltage drop are imminent, it is negligible compared to the voltage drop of the lines. The shunt path has a very high impedance. Hence, during normal period, total line current flows through the bridge except very small amount of leakage current flowing through the shunt path. When faults occur, there is a rapid increase of line current, but the L_{dc} suppresses this rapid increase of line current di/dt for the safety of the IGBT [25], [35], [36], [39]–[41].

C. NEURO FUZZY LOGIC CONTROLLER FOR PRFCL

The per-phase configuration of the NFLC for PRFCL is shown in Fig. 6. The one-fourth cycle delay of the instantaneous phase voltage, $V_{inst,\phi}$ or $V_{d,\phi}$ is taken to produce a quadrature component, $V_{q,\phi}$. $V_{dq,\phi}$ is then calculated by the following expression:

$$V_{dq,\phi} = \sqrt{V_{d,\phi}^2 + V_{q,\phi}^2} \tag{21}$$

The $V_{dq,\phi}$ is constantly compared with a reference voltage, V_{ref} and the difference between $V_{dq,\phi}$ and V_{ref} is used as the input of the NFLC. The NFLC produces the duty cycle, d that works as the control input of the IGBT. Since the impedance inserted at the time of fault instance should not be very small, d is always kept between 0.5 and 1. To detect the fault, a threshold voltage, $V_{th} = 0.9$ pu is compared with the $V_{dq,\phi}$. The difference between $V_{dq,\phi}$ and V_{th} is sent to a selector that switches between two logic levels. At normal operating condition ($V_{dq,\phi} > V_{th}$), the selector selects "b" that sends HIGH signal to the IGBT and during fault ($V_{dq,\phi} < V_{th}$), it selects "a" which is the inverted output of the PWM generator. But, instead of applying the full impedance of the shunt path during the entire fault period, a variable effective shunt impedance, $Z^*_{shunt} = d \times Z_{shunt}$ is provided to the system for flexible compensation by the NFLC-PRFCL, where Z_{shunt}

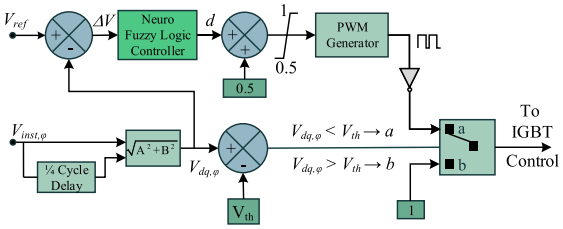

FIGURE 6. Per phase neuro fuzzy logic controller.

denotes the shunt impedance and d is the duty ratio generated by the NFLC defined by the following expression:

$$d = \frac{T_{off}}{T_c} \tag{22}$$

where T_c is the total time period of the PWM output and T_{off} is the time for which the IGBT does not conduct. T_c can be defined as, $T_c = T_{off} + T_{on}$. Here T_{on} is the time for which the IGBT of the diode bridge conducts. The variable shunt impedance Z^*_{shunt} provides flexibility to the NFLC-PRFCL and makes it dynamically respond to the severity level of the faults.

D. NEURO FUZZY LOGIC CONTROLLER DESIGN

The design of NFLC for PRFCL is discussed in the following subsections.

1) STRUCTURE OF NEURO FUZZY INFERENCE SYSTEM

Adaptive neuro fuzzy inference system (ANFIS) is mainly implemented as teaching method for a sugeno fuzzy inference system (FIS) [51]. Sugeno system is more effective than the mamdani system [42], [43]. ANFIS allows us to design the parameters of the fuzzy membership function (MF) based on the practical data automatically using back propagation or hybrid method [42]. Some optimization techniques known as the sum of squared differences between the practical values and the target values are used for controlling the parameters of the MF. The structure of ANFIS is shown in Fig. 7. Every node in the first layer is for a linguistic variable and the output generates the grade of the MF. Input signals are multiplied in each node of the second layer and the product corresponds to the firing strength (W_i) of a rule [43]. Every node represented in the third layer is for calculating the ratio of the firing strength of i_{th} rule to the sum of total firing strength. Nodes on the fourth layer (output MF) give the output by multiplying the rule f_i with the relative firing strength of i_{th} rule. Fifth layer is for final output which is achieved by summing the incoming signals from layer 4 [43].

2) DESIGN OF NEURO FUZZY INFERENCE SYSTEM

The difference between the reference voltage, V_{ref} and the dq voltage, $V_{dq,\phi}$, ΔV is used as an input of the ANFIS controller and the duty cycle, d is its output. This single input and single output variable make the controller very simple in design. ANFIS editor display is divided into four main sub-displays:

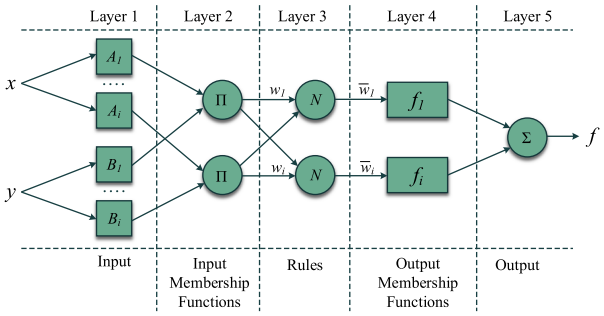

FIGURE 7. Structure of ANFIS.

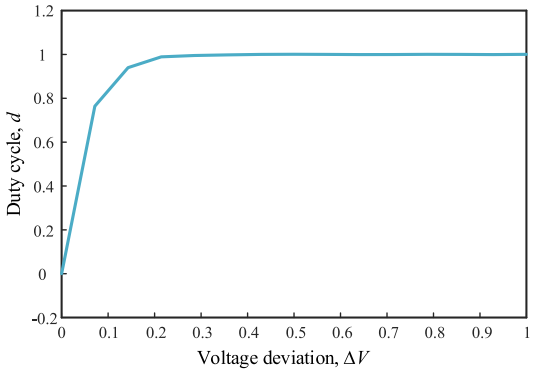

FIGURE 8. Surface view of the designed neuro fuzzy inference system.

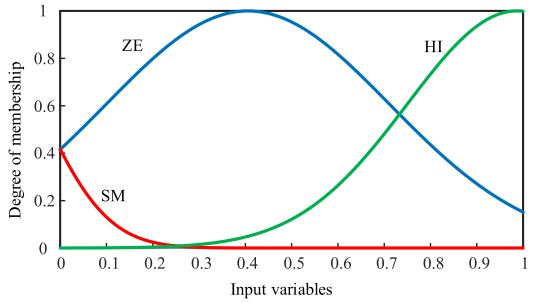

FIGURE 9. Input membership function of neuro fuzzy inference system.

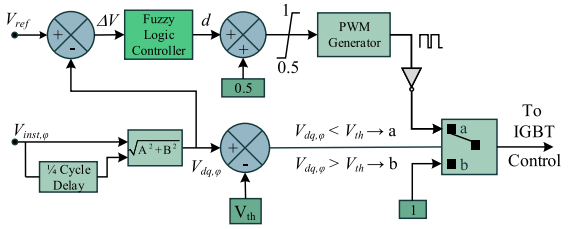

FIGURE 10. Per phase fuzzy logic controller.

1) Loading of data: First, we have generated the training data set from which we have to generate the MF. Training data was generated by linearly dividing the input variable, ΔV and estimating its corresponding output variable, d. The data was taken as a 1-D input vector and 1-D output vector in matrix form.
2) Generation of the FIS: The next work is to generate an initial "fuzzy inference system" file using the "Generate FIS" in the ANFIS GUI in MATLAB. The Gaussian MFs provided the best performance for controlling the PRFCL. Grid partitioning was used to generate the "fuzzy inference system" file. As there are only three MFs, grid partitioning is more accurate and requires less time.
3) Training the FIS: The main part of designing the ANFIS is to train the FIS. Hybrid algorithm was used [42] to fit the data with the number of epochs of 100. The hybrid optimization method uses both the least-squares and back propagation algorithms to learn the parameter of the MFs used previously [52]. The model is trained until the error is minimum. Initially, the error tolerance was zero but it is not practically possible. So this parameter was changed to 0.001.
4) Testing the FIS: Finally, we tested the performance of our FIS using some relevant testing data which were taken in the same way we collected the training data.

The ANFIS editor toolbox in MATLAB/Simulink is used here for the above process. The number of data pairs that were collected to train the plant was 26. From the surface view of the designed ANFIS shown in Fig. 8, it is seen that the input can be varied from 0 to 0.9999 per unit and the corresponding value of output d varies from 0 to 1. It provides another information that the larger the deviation in the PCC voltage, the greater the value of the duty cycle d. The input MF of the ANFIS controller is shown in Fig. 9.

If the wind speed changes, the operation of the proposed controller might get affected accordingly [39]. But, as the fault or transient situation is the only consideration here, it can be assumed that the wind speed is constant during this short time period [39].

E. FUZZY LOGIC CONTROLLER DESIGN FOR PRFCL

To understand the superiority of the NFLC-PRFCL, its performance is also compared with that of the existing FLC-PRFCL [39]. The design of FLC-PRFCL is discussed in the following subsections:

1) DESIGN OF MEMBERSHIP FUNCTIONS

In the fuzzy logic controller, the input of the controller is the deviation between the instantaneous dq voltage of the PCC, $V_{dq,\phi}$ and the reference voltage, V_{ref}, denoted as ΔV. The output of the controller is the duty cycle, d, which controls the PWM generator. The per phase fuzzy logic control scheme is shown in Fig. 10.

For designing the MFs, Gaussian MFs for input ΔV and output d are shown in Fig. 11 and Fig. 12 respectively. The Gaussian MFs provide better convergence than other MFs [39]. The linguistic variables ZE, SM, HI, MB, and BI means zero, small medium, high, medium big and big, respectively.

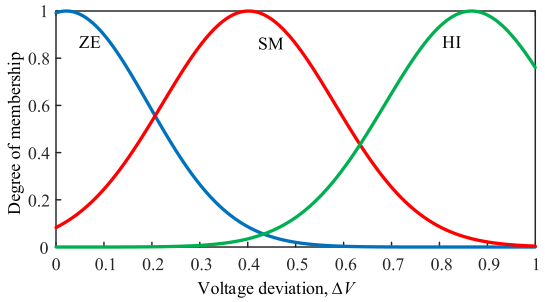

FIGURE 11. Input membership function of fuzzy logic controller.

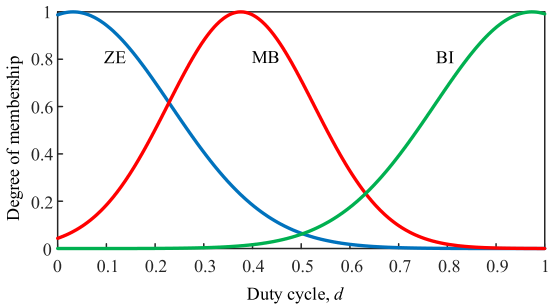

FIGURE 12. Output membership function of fuzzy logic controller.

TABLE 1. Fuzzy rule base.

PCC voltage deviation, ΔV	Duty cycle, d
ZE	ZE
SM	MB
HI	BI

According to the operating point of the wind farm, the MFs were tuned to get the best performance. The equation describing the Gaussian MFs is [39]:

$$f(x;\sigma,c) = e^{-\frac{x-c}{2\sigma^2}} \tag{23}$$

where σ and c is the width of the bell curve and the center of the peak respectively.

2) RULE BASE

Fuzzy rules are used within fuzzy logic systems to infer an output based on input variable. Here, the system comprises only one input and one output, which made the fuzzy controller very simple [53]. The rules were designed according to the practical viewpoint as shown in the Table 1.

3) FUZZY INFERENCE

Fuzzy inference system is the process of mapping the output from a given input with the help of fuzzy logic. Mamdani fuzzy inference system is a process in which the control system is designed by combining all the linguistic rules which are taken from human operators. In this inference system, the degree of conformity, W_i is as follows [39]:

$$W_i = \mu_i(\Delta V) \tag{24}$$

here i is called the rule number.

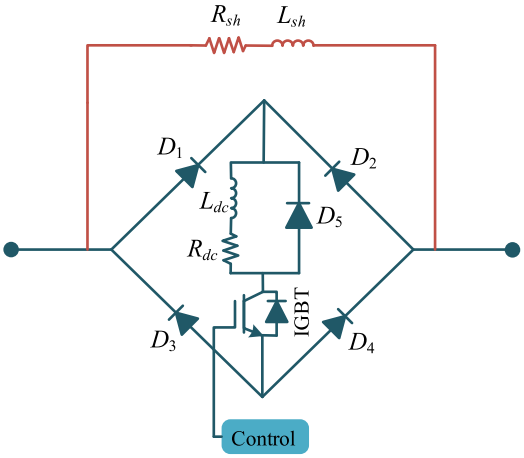

FIGURE 13. Architecture of the BFCL.

4) DEFUZZIFICATION

Defuzzification is the mapping of output crisp value from the corresponding fuzzy sets and membership degrees. There are a number of rules to transform the fuzzy sets to corresponding crisp set. The most useful one is the center of gravity method and it is implemented to determine the output according to the following expression [39]:

$$d = \frac{\int z.\mu_i(z)dz}{\int \mu_i(z)dz} \tag{25}$$

here d corresponds to the value of $\mu_i(z)$ which is the fuzzy linguistic variable.

V. BRIDGE-TYPE FAULT CURRENT LIMITER (BFCL) AND SERIES DYNAMIC BRAKING RESISTOR (SDBR)

Since the performance of the proposed NFLC-PRFCL will be compared and analyzed with that of the BFCL and SDBR, it is necessary to discuss their constructions and control structures. The discussions are provided in the following subsections.

A. BRIDGE-TYPE FAULT CURRENT LIMITER

1) CONSTRUCTION OF THE BFCL

Description, operation principle, and topology of the BFCL have been discussed in the previous works [34], [44], [49]. The BFCL comprises with two distinctive parts as presented in Fig. 13. However, the main part of the BFCL is a typical bridge circuit with four diodes (D_1-D_4). The other part is a shunt path which consists of an inductor (L_{sh}) along with a series resistor (R_{sh}). Apart from these, inside the bridge, an IGBT switch is included in series with an inductor (L_{dc}). The intrinsic resistance (R_{dc}) of the L_{dc} is of very negligible magnitude. However, to protect the DC reactor from a sudden inrush current during the fault condition, a free-wheeling diode (D_5) is connected in parallel with the (L_{dc}).

2) WORKING PRINCIPLE OF THE BFCL

Under normal operating conditions of the BFCL, during positive and negative half cycles, the current will pass through

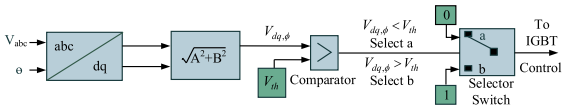

FIGURE 14. Control scheme of the BFCL and the SDBR.

TABLE 2. Parameters of the BFCL.

R_{sh}	L_{sh}	R_{dc}	L_{dc}
20 Ω	250 mH	0.003 Ω	1 mH

the paths D_1-L_{dc}-R_{dc}-$IGBT$-D_4 and D_3-$IGBT$-R_{dc}-L_{dc}-D_2, respectively. At the event of the fault, the IGBT switch turns off due to control actions and the shunt impedance comes in series to limit the effect of fault current. After the removal of the fault, the IGBT switch turns on again and the BFCL resumes its normal operation [34], [44], [49]. The control scheme for the existing BFCL is presented in the following subsection.

3) CONTROL SCHEME FOR THE BFCL

For the BFCL, the instantaneous voltage of the PCC is considered as the input which can be clearly seen from Fig. 14. During normal operating condition, the value of $V_{dq,\phi}$ is continuously monitored and compared with a reference threshold value, V_{th}. A HIGH state gate pulse signal will be supplied to the gate of the IGBT switch when the difference between the $V_{dq,\phi}$ and V_{th} is positive. During normal operation, the shunt path will be inactive. However, when a fault occurs on the system, the value of $V_{dq,\phi}$ will be significantly reduced and the difference between $V_{dq,\phi}$ and V_{th} becomes negative. At this stage, a LOW state gate pulse signal will be supplied to the gate of the IGBT switch and consequently, it will be turned off. This will make the bridge circuit open and the fault current gets diverted through the shunt path. However, the high resistance and inductance of the shunt path cease the fault current to a considerable limit and stabilize the system quickly afterward [35], [39], [49].

4) DESIGN CONSIDERATION OF THE BFCL

The designed parameters of the BFCL are listed in Table 2. In order to select the values of R_{sh}, L_{sh}, R_{dc} and L_{dc}, a detailed analysis is presented in [34] and in our previous work [37]. As the performance of the proposed method is also compared with the SDBR, the construction and operating principle of the SDBR are discussed in the following subsections.

B. SERIES DYNAMIC BRAKING RESISTOR

1) CONSTRUCTION OF THE SDBR

The SDBR is a well-known technique and according to literature, it has the potential to augment the FRT capability of wind generation systems [32], [33]. It has a resistor in parallel with a switch as shown in Fig. 15. In this study, an IGBT is used as a switch due to its special features such as quick response and compatible design.

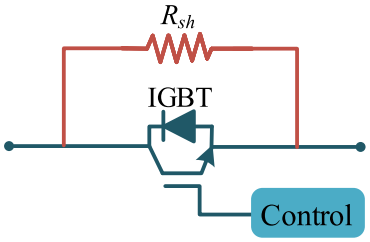

FIGURE 15. Architecture of the SDBR.

2) WORKING PRINCIPLE OF THE SDBR

The gate pulses of the IGBT are controlled according to the control system described in the previous section and as depicted in Fig. 14. During the normal operating mode, the IGBT switch of the SDBR remains closed and the line current flows through it as the IGBT switch gets a HIGH signal. However, when a fault occurs in the system, the line current will be sharply increased and the controller will send a LOW signal to the gate of the IGBT and consequently, the IGBT will be turned off. In this condition, the line current will flow through the available shunt path [32], [33]. In order to make a fair comparison, the value of the braking resistor is kept identical to the BFCL as listed in Table 2.

VI. SIMULATION RESULTS AND DISCUSSIONS

In this section, the performance of the NFLC-PRFCL is evaluated on the system as shown in Fig. 4, which is implemented in the MATLAB/Simulink environment using the Simpower ToolBox. All simulation parameters are listed in Table 12 of the Appendix. In order to show the effectiveness of the proposed NFLC-PRFCL, two types of faults such as, temporary and permanent faults are considered in this work, which is applied at the point F of the considered system model as shown in Fig. 4. In order to demonstrate the superiority of the proposed method, its performance is compared with that of the SDBR [32], [33], BFCL [34], [44] and FLC-PRFCL [39]. Detailed simulation results under both scenarios are discussed in the following subsections.

A. SYSTEM RESPONSES UNDER TEMPORARY FAULTS

In this case study, both symmetrical (three-line-to-ground-3LG, which is the most severe faults on power systems) and unsymmetrical (single-line-to-ground-1LG, which is the most common fault on power systems) faults are considered which occurs at t = 0.1 s. Both faults are applied for 100 ms and then the circuit breakers (CBs) of the faulty line are opened at t = 0.2 s to clear the fault and then reclosed at t = 1.2 s [34], [37]. The system responses corresponding to both symmetrical and unsymmetrical faults along with a discussions are presented in the following subsections.

1) SYSTEM RESPONSE WITH SYMMETRICAL FAULT

System responses during a temporary symmetrical fault are shown Fig. 16 to Fig. 23. Without any auxiliary FCL, the voltage response at the PCC reaches zero as soon as the fault is

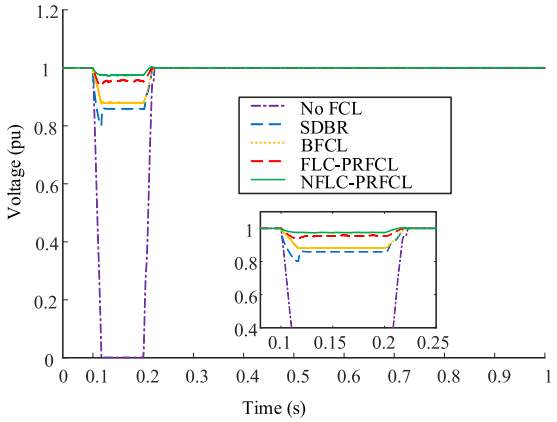

FIGURE 16. Voltage response at the PCC for temporary 3LG fault.

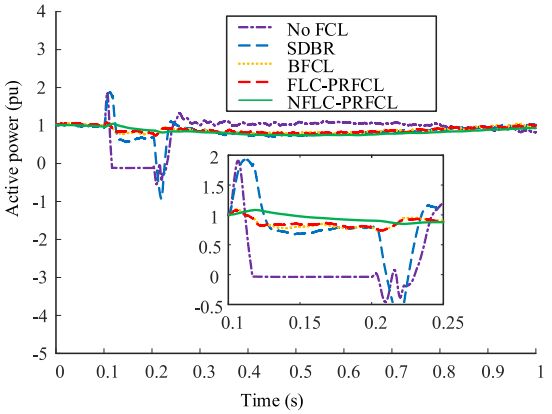

FIGURE 17. Active power response at the PCC for temporary 3LG fault.

initiated. The voltage stays at zero as long as the CBs on the faulty line are in closed mode and it starts recovering after the opening of those CBs. The voltage response improves significantly after the FCLs are introduced to the system. The SDBR, BFCL and FLC-PRFCL, all did very well to reduce the voltage sag during the fault. However, the NFLC-PRFCL resulted the lowest sag and minimum oscillations. Also, it assured faster recovery to prefault voltage level compared to the FLC-PRFCL, BFCL and SDBR as shown in Fig. 16.

The active power at the PCC generally reduces significantly during the fault period. However, without any FCL on the system, the active power at the PCC becomes very low which can be clearly seen from Fig. 17. There is a sudden rise of the active power due to the mismatch between the extracted and the demanded wind power at the instant of opening of the CBs. Though the existing SDBR, BFCL, and FLC-PRFCL are able to minimize certain power fluctuations, the proposed NFLC-PRFCL can control this in a better way. Consequently, the NFLC-PRFCL shows minimum amount of power fluctuations and sag which can be clearly observed from Fig. 17. Similarly, the reactive power at the PCC shown in Fig. 18 has the lowest oscillations when the NFLC-PRFCL is used, whereas the existing FCLs resulted in more oscillations and sag. Also, from Fig. 18 it can be seen that the proposed

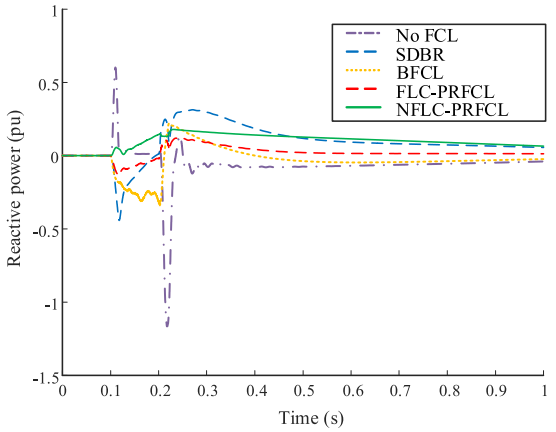

FIGURE 18. Reactive power at the PCC for temporary 3LG fault.

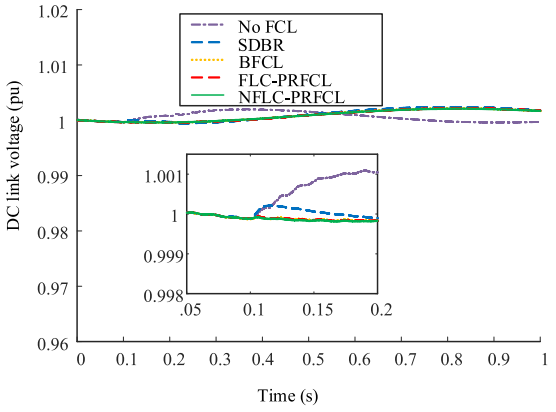

FIGURE 19. DC-link voltage response for temporary 3LG fault.

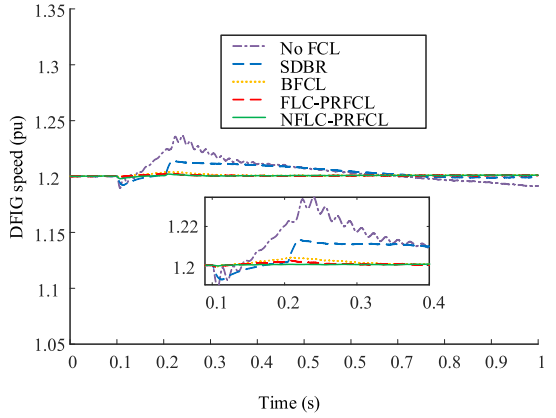

FIGURE 20. Speed response of the DFIG for temporary 3LG fault.

NFLC-PRFCL can assure a constant reactive power supply during the fault period to compensate for the voltage dip while enhancing the system stability.

The DC-link voltage response of the DFIG associated with the WT#1 is shown in Fig. 19. It can be observed that the traditional FCLs (SDBR and BFCL) can maintain a constant DC-link voltage within the reference level. Though the DC-link voltage is constant at the reference voltage, there are some fluctuations. On the other hand, the FLC-PRFCL

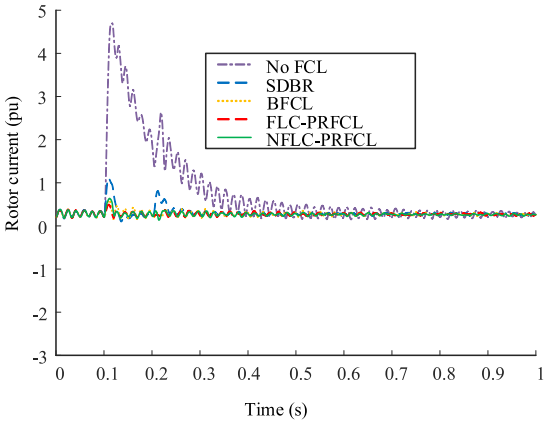

FIGURE 21. Rotor current for temporary 3LG fault.

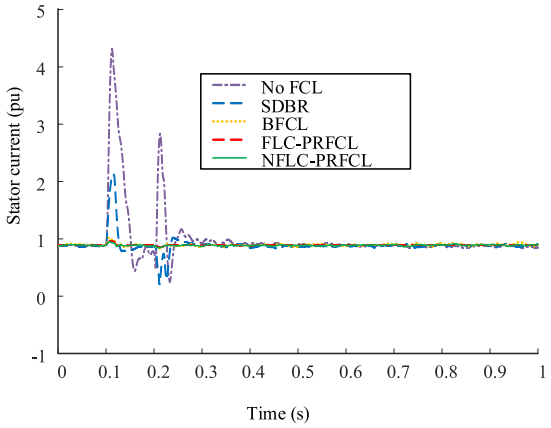

FIGURE 22. Stator current for temporary 3LG fault.

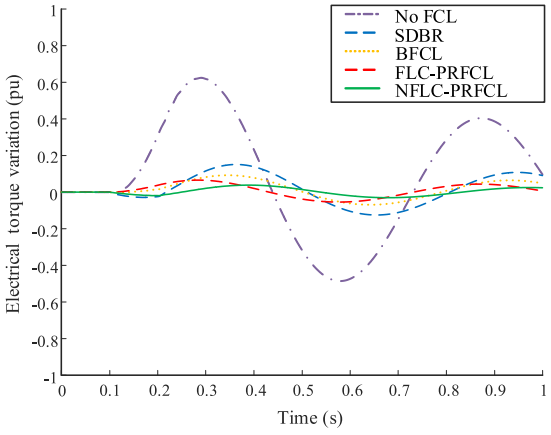

FIGURE 23. Electrical torque variations of DFIG for temporary 3LG fault.

and the proposed NFLC-PRFCL are capable of keeping the DC-link voltage at a constant level with least fluctuations. However, among these two schemes, the proposed NFLC-PRFCL can provide a better result as compared to the FLC-PRFCL which can be clearly seen from Fig. 19. It is well-known that during any fault on the DFIG-based power system, the speed of the DFIG will be suddenly increased at the instant of the fault and after certain time period, it will restore to the pre-fault speed level. This phenomenon is clearly reflected in this case study as well and can be clearly seen from Fig. 20. During fault, the speed deviation is severe when there is no FCL. On the other hand, the speed deviation is significantly reduced when a FCL is used which is prominent from Fig. 20. However, the speed deviation is the lowest with the proposed NFLC-PRFCL as compared to the SDBR, the BFCL and the FLC-PRFCL. The corresponding rotor and stator currents are depicted in Fig. 21 and Fig. 22, respectively. From these figures, it is clear that the FLC-PRFCL has lower current rise in comparison with the SDBR and the BFCL but the proposed NFLC-PRFCL has the lowest current rise with minimum fluctuations.

Fig. 23 illustrates the electrical torque variations of DFIG for 3LG fault. Without any FCL, the DFIG experiences maximum amount of torque variations. The torque variation can reach as much as 0.6 pu in case of no FCL. The SDBR, the BFCL and the FLC-PRFCL can limit the torque variation upto a certain level, but the NFLC-PRFCL can keep the torque variation to the minimum and can reach the steady state value much faster than the other adopted strategies.

From the above analysis, it is evident that the proposed NFLC-PRFCL is the best choice for improving the system performances as compared to other existing methods. The performance of the proposed NFLC-PRFCL is also analyzed for the unsymmetrical fault which is discussed in the following subsection.

2) SYSTEM RESPONSES WITH UNSYMMETRICAL FAULT

In power systems, the asymmetrical fault is more common than a three-phase fault. Therefore, in this case study, simulations are also carried out when an unsymmetrical fault is occurred on the system. The fault occurrence sequence as well as the opening and closing of the CBs are maintained in a similar manner as described in the previous subsection. The corresponding simulation results of a grid-connected DFIG-based wind firm have been shown from Fig. 24 to Fig. 31. Fig. 24 represents the simulated PCC voltage, from where it can be observed that without any FCL, the voltage goes to around 60% of the pre-fault level and recovers after opening the CBs. The FLC-PRFCL outperforms both the BFCL and the SDBR in all aspects. But from the zoom view of the PCC voltage response, it clearly indicates that the proposed NFLC-PRFCL has the lowest perturbation with minimum amount of sags as compared to all existing schemes. The active and reactive power profiles of the PCC for a 1LG fault are shown in Fig. 25 and Fig. 26, respectively. From these figures, it is evident that there are certain amount of power deviations for all schemes. However, the proposed NFLC-PRFCL shows better performance by keeping the oscillations in a lowest level while maintaining a fairly smooth reactive power during and after clearing the fault. Due to this fault, the DC-link voltage has no sudden rise which can be seen from Fig. 27. However, the proposed NFLC-PRFCL

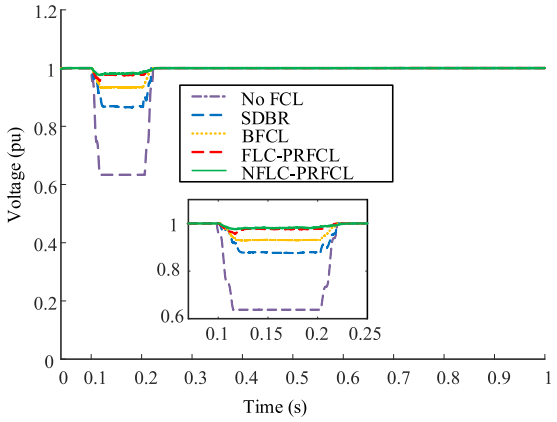

FIGURE 24. Voltage response at the PCC for temporary 1LG fault.

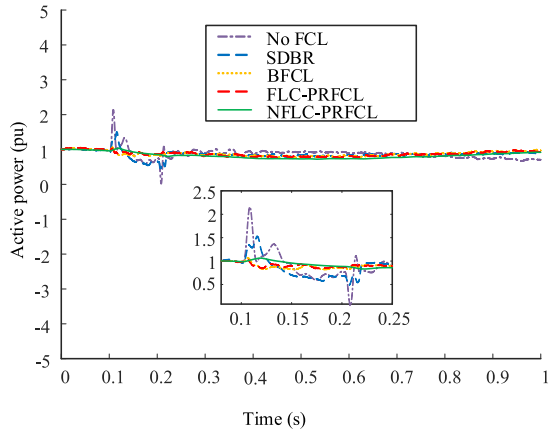

FIGURE 25. Active power response at the PCC for temporary 1LG fault.

can hold the DC-link voltage within a minimum fluctuation level as compared to other schemes.

The speed response of a DFIG at WT#1 is illustrated in Fig. 28. From the figure, it can be seen that for the FLC-PRFCL, the speed has less fluctuations than that of the BFCL and the SDBR. However, the proposed NFLC-PRFCL assured the best response exhibiting the least oscillations in speed. Similarly, from the rotor and stator current responses as shown in Fig. 29 and Fig. 30 respectively, it can be observed that these currents are subdued to a minimum level in a better way when NFLC-PRFCL is used compared to the existing methods. The electrical torque variations of DFIG during a temporary 1LG fault is displayed in Fig. 31. Similar to the temporary 3LG fault, the best response is obtained for NFLC-PRFCL as it keeps the torque variation minimum and has lower settling time. An index-based analysis for the temporary fault is also presented in this work which is discussed in the following subsection.

3) INDEX-BASED ANALYSIS FOR TEMPORARY FAULT

In order to verify the superiority of the proposed method numerically, an index-based comparison is also carried out to find out the performance index of each FCL as presented

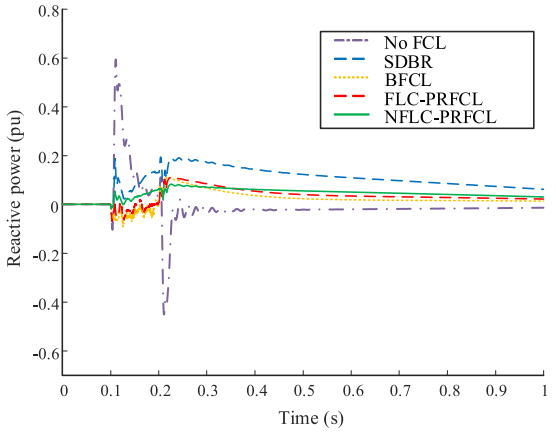

FIGURE 26. Reactive power at the PCC for temporary 1LG fault.

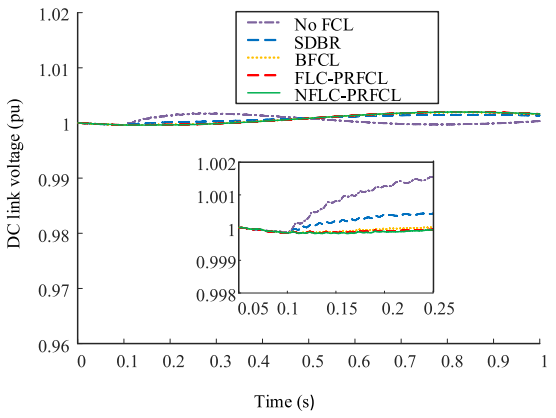

FIGURE 27. DC-link voltage response for temporary 1LG fault.

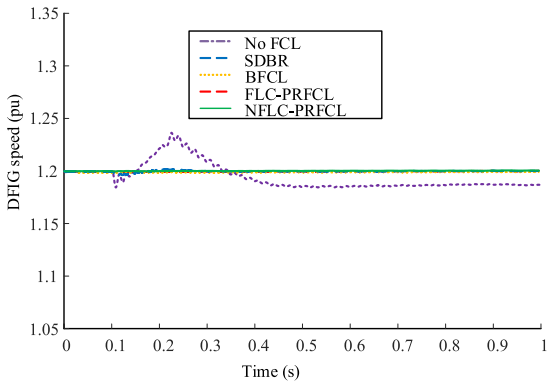

FIGURE 28. Speed response of the DFIG for temporary 1LG fault.

in [34], [39], [49]. In this analysis, the indices are entitled as *vlt*(*pu.s*), *pow*(*pu.s*), *reactive*(*pu.s*), *dclink*(*pu.s*), *spd*(*pu.s*), *rtr*(*pu.s*), *str*(*pu.s*) and *torque*(*pu.s*) and they are calculated based on following mathematical definitions:

$$vlt(pu.s) = \int_0^T \mid \Delta V \mid dt \tag{26}$$

$$pow(pu.s) = \int_0^T \mid \Delta P \mid dt \tag{27}$$

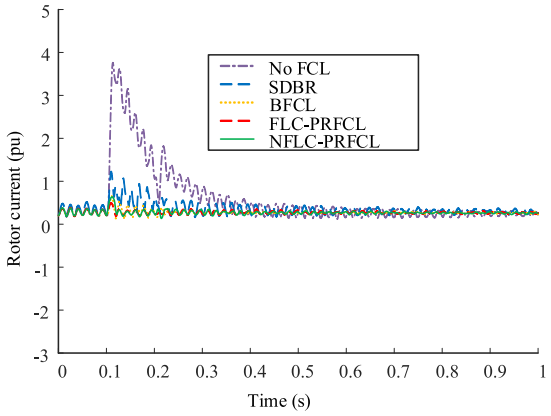

FIGURE 29. Rotor current for temporary 1LG fault.

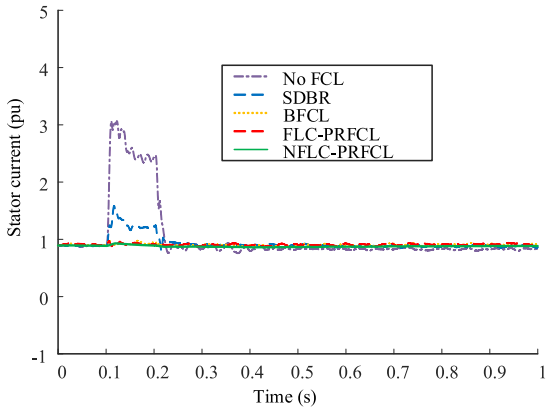

FIGURE 30. Stator current for temporary 1LG fault.

$$reactive(pu.s) = \int_0^T \mid \Delta Q \mid dt \tag{28}$$

$$dclink(pu.s) = \int_0^T \mid \Delta V_{dc} \mid dt \tag{29}$$

$$spd(pu.s) = \int_0^T \mid \Delta \omega \mid dt \tag{30}$$

$$rtr(pu.s) = \int_0^T \mid \Delta I_r \mid dt \tag{31}$$

$$str(pu.s) = \int_0^T \mid \Delta I_s \mid dt \tag{32}$$

$$torque(pu.s) = \int_0^T \mid \Delta \tau \mid dt \tag{33}$$

where ΔV, ΔP, ΔQ, ΔV_{dc}, $\Delta \omega$, ΔI_r, ΔI_s and $\Delta \tau$ are the deviations of the PCC voltage, active power, reactive power, DC-link voltage, generator speed, rotor current, stator current, and electrical torque variations respectively. To measure the indices, a time interval, T is considered in this work, which is varied from 0 to 1 s for a temporary fault. Since the performance indices are calculated based on the deviation, the lower value of indices indicates the better FRT performance of the wind generator. The performance indices for the symmetrical and unsymmetrical faults are listed in Table 3 and Table 4, respectively.

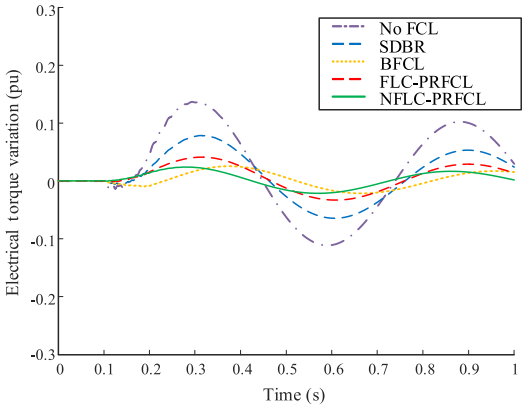

FIGURE 31. Electrical torque variations for temporary 1LG fault.

TABLE 3. Performance indices for temporary symmetrical (3LG) fault.

Index parameters (%)	Values of indices				
	No FCL	SDBR	BFCL	FLC-PRFCL	NFLC-PRFCL
vlt(pu.s)	10.145	1.614	1.241	0.563	0.294
pow(pu.s)	27.327	12.281	7.151	2.223	2.081
reactive(pu.s)	10.363	9.833	7.238	6.034	5.265
dclink(pu.s)	0.112	0.037	0.034	0.017	0.016
spd(pu.s)	0.869	0.442	0.101	0.014	0.009
rtr(pu.s)	46.838	4.739	2.135	1.843	1.071
str(pu.s)	21.706	18.148	2.655	1.540	1.055
torque(pu.s)	27.840	6.888	4.117	3.038	1.735

TABLE 4. Performance indices for temporary unsymmetrical (1LG) fault.

Index parameters (%)	Values of indices				
	No FCL	SDBR	BFCL	FLC-PRFCL	NFLC-PRFCL
vlt(pu.s)	3.982	1.314	0.670	0.235	0.227
pow(pu.s)	11.808	8.483	3.057	1.880	1.344
reactive(pu.s)	9.034	4.275	3.565	3.387	2.543
dclink(pu.s)	0.101	0.036	0.031	0.027	0.024
spd(pu.s)	0.291	0.086	0.058	0.024	0.016
rtr(pu.s)	34.220	3.245	1.754	0.854	0.731
str(pu.s)	18.462	6.977	2.006	0.799	0.695
torque(pu.s)	6.370	3.585	1.924	1.173	1.149

From Table 3 and Table 4, it can be seen that all the performance indices are maximum when there is no FCL. In case of the FLC-PRFCL, the indices values are quite smaller than the SDBR and the BFCL. However, for the proposed NFLC-PRFCL, the values of the indices are the least among the three existing schemes. This is true for both symmetrical and unsymmetrical faults. Since the performance of any FCL is inversely related to its corresponding percentage indices, therefore, it can be concluded that the proposed NFLC-PRFCL can enhance the system stability in a better way compared to other existing methods.

4) QUANTITATIVE ANALYSIS AT STEADY-STATE CONDITIONS OF THE SYSTEM UNDER TEMPORARY FAULTS

In this section, a quantitative analysis of the system under temporary faults is presented in order to prove the

TABLE 5. Steady state analysis for temporary symmetrical (3LG) fault.

FCLs	Percentage overshoot						Settling time (s)					
	Active power	DC-link voltage	DFIG speed	Rotor current	Stator current	Torque	Active power	DC-link voltage	DFIG speed	Rotor current	Stator current	Torque
No FCL	44.884	0.133	2.158	95.150	79.424	96.797	12.838	∞	16.915	4.754	1.744	19.846
SDBR	43.531	0.051	0.967	76.859	55.683	86.764	0.645	2.562	5.334	0.581	0.935	13.267
BFCL	8.263	0.048	0.210	36.387	6.798	78.341	0.178	1.079	0.134	0.572	0.585	8.146
FLC-PRFCL	5.903	0.034	0.056	25.455	2.213	69.866	0.098	0.528	0.043	0.478	0.539	5.176
NFLC-PRFCL	5.193	0.031	0.042	21.468	1.547	47.930	0.089	0.493	0.035	0.340	0.292	2.944

TABLE 6. Steady state analysis for temporary unsymmetrical (1LG) fault.

FCLs	Percentage overshoot						Settling time (s)					
	Active power	DC-link voltage	DFIG speed	Rotor current	Stator current	Torque	Active power	DC-link voltage	DFIG speed	Rotor current	Stator current	Torque
No FCL	53.405	0.132	2.049	93.685	71.016	85.380	11.252	12.984	15.192	2.975	0.974	12.276
SDBR	34.248	0.049	0.474	83.028	51.382	74.535	0.506	4.168	0.269	0.395	0.751	6.016
BFCL	10.029	0.048	0.032	49.288	9.374	51.362	0.456	0.934	0.066	0.273	0.418	3.487
FLC-PRFCL	8.267	0.041	0.027	43.203	8.178	21.661	0.062	0.519	0.041	0.196	0.317	3.148
NFLC-PRFCL	5.167	0.039	0.022	32.190	7.342	16.943	0.048	0.468	0.031	0.181	0.224	1.944

effectiveness of the proposed NFLC-PRFCL. The quantitative analysis in terms of percentage overshoot and settling time of the system responses is carried out for both symmetrical and unsymmetrical faults, which are listed in Table 5 and Table 6, respectively. The voltage responses at the PCC are excluded from the analysis as they do not exhibit any overshoot for any of the FCLs we used in this work. Table 5 represents the quantitative results of different FCLs for a temporary symmetrical-3LG fault, from where it can be seen that the percentage overshoot and the settling time without any FCL are the highest for all system responses. But, after installing FCLs, these values are significantly reduced. However, these values are quite smaller for NFLC-PRFCL as compared to the SDBR, BFCL, and FLC-PRFCL which prove the superiority of the proposed scheme. Similarly, for a temporary unsymmetrical-1LG fault, the proposed NFLC-PRFCL shows a better improvement than the existing methods which can be clearly observed from the data as provided in Table 6.

B. SYSTEM RESPONSES UNDER A PERMANENT FAULT

In this section, the performance of the proposed NFLC-PRFCL is analyzed for 3LG and 1LG permanent faults which occur at the point F in Fig. 4. Both faults occur at t = 0.1 s and continues for an indefinite time. The CBs on the faulty lines are opened at t = 0.2 s and reclosed again at t = 1.2 s. However, the fault still persists at t = 1.2 s and due to that, an unsuccessful reclosure of the CBs take place. Therefore, the CBs are opened once again at t = 1.3 s and remain open because of the permanent fault.

The corresponding system responses for 3LG and 1LG permanent faults are illustrated in Fig. 32 to Fig. 47. From these

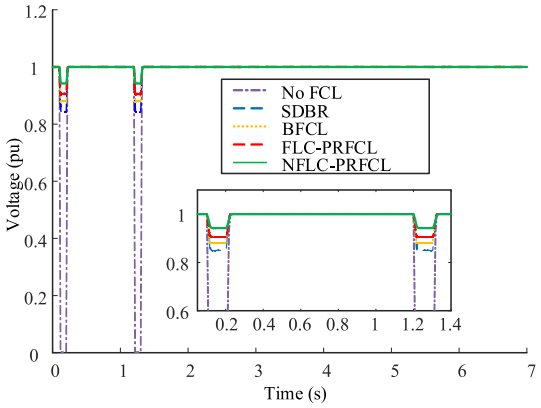

FIGURE 32. Voltage response at the PCC for permanent 3LG fault.

figures, it can be noticed that the FLC-PRFCL performs in a better way compared to the SDBR and BFCL. However, the proposed NFLC-PRFCL outperforms all these existing methods. Therefore, analyzing the results, it can be concluded that the NFLC-PRFCL is the best candidate during permanent faults to augment the FRT capability of DFIG based wind farms. For this permanent fault, an index-based analysis is also carried out which is discussed in the following subsection.

1) INDEX-BASED ANALYSIS FOR PERMANENT FAULT

Performance indices of the system responses for different FCLs under both symmetrical and unsymmetrical faults are shown in Table 7 and Table 8, respectively. Similar to the temporary fault analysis, the indices of the system responses

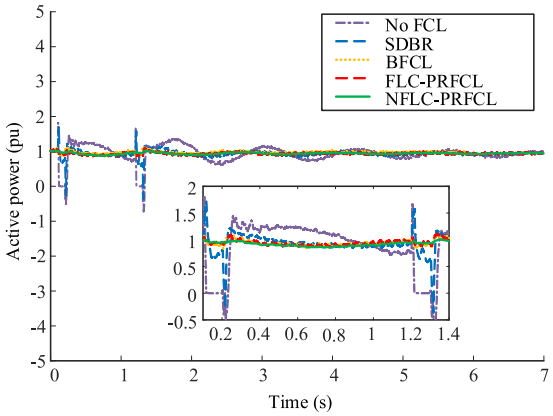

FIGURE 33. Active power response at the PCC for permanent 3LG fault.

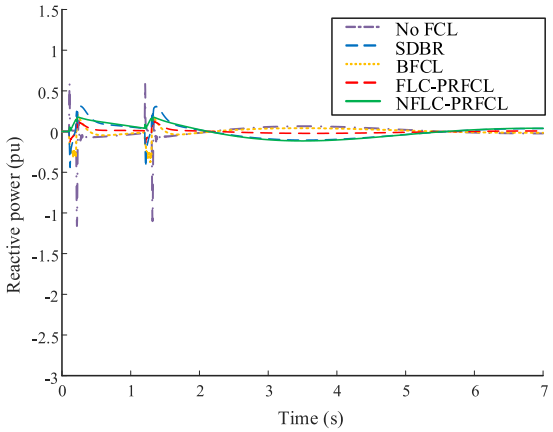

FIGURE 34. Reactive power at the PCC for permanent 3LG fault.

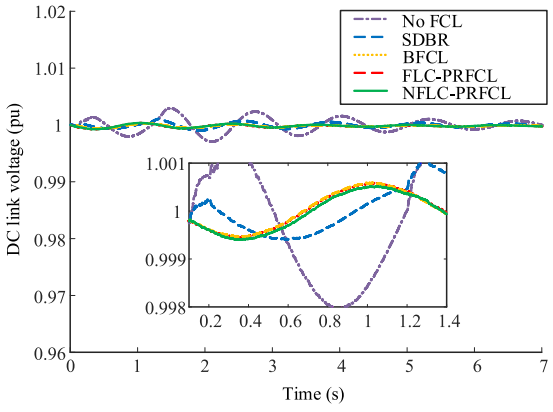

FIGURE 35. DC link voltage response for permanent 3LG fault.

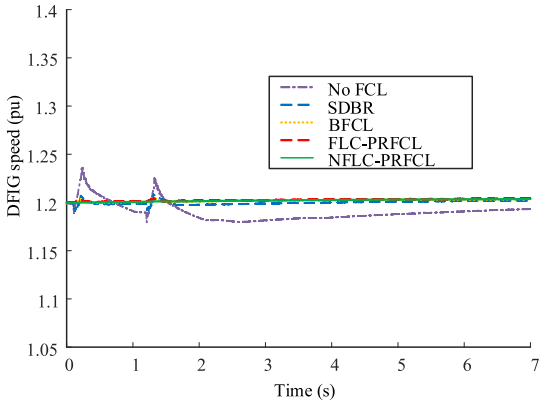

FIGURE 36. Speed response of the DFIG for permanent 3LG fault.

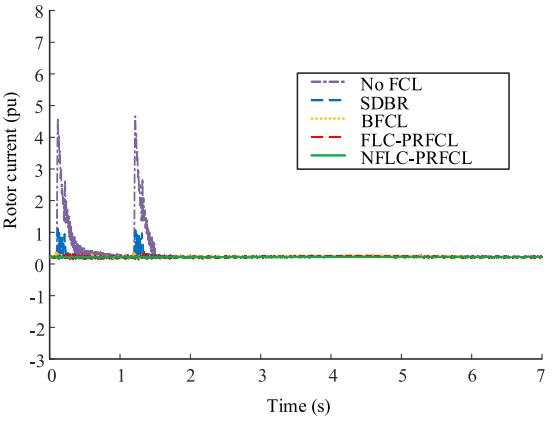

FIGURE 37. Rotor current for permanent 3LG fault.

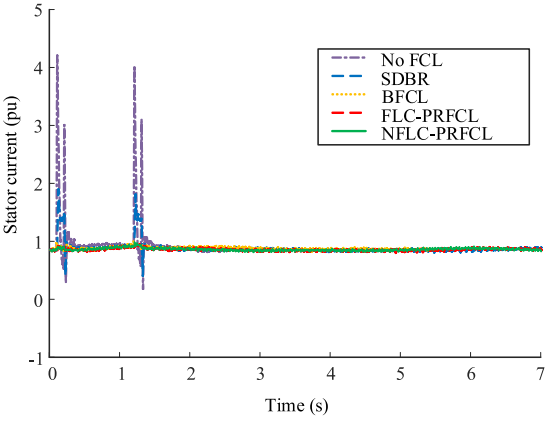

FIGURE 38. Stator current for permanent 3LG fault.

under permanent faults also demonstrate the superiority of the proposed NFLC-PRFCL.

2) QUANTITATIVE ANALYSIS AT STEADY-STATE CONDITIONS OF THE SYSTEM UNDER PERMANENT FAULTS

The quantitative analysis at steady-state conditions of the system under permanent symmetrical and unsymmetrical faults are shown in Table 9 and Table 10, respectively. It is noted that for this analysis, two different cases are considered i.e., when CBs open for the first time and when the CBs open again due to unsuccessful re-closure due to the persistent of the fault. From these tables, it can be observed that the percentage overshoot is the lowest for all responses when the proposed NFLC-PRFCL is used, whereas for other existing methods, these values are quite high. For some responses, the calculation of the settling time is not possible after the

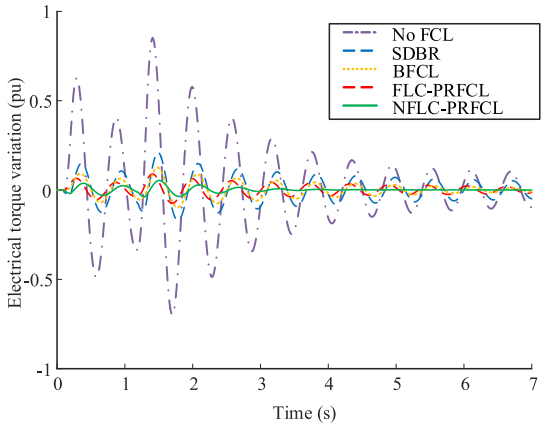

FIGURE 39. Electrical torque variations for permanent 3LG fault.

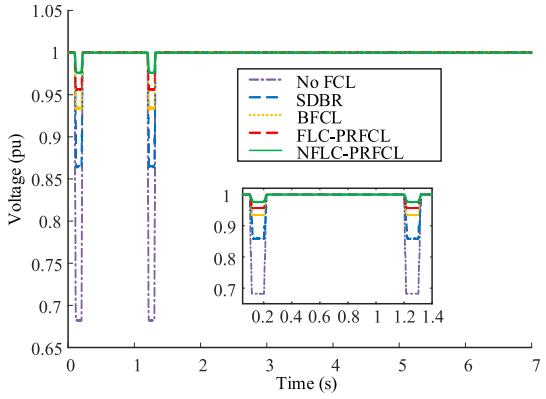

FIGURE 40. Voltage response at the PCC for permanent 1LG fault.

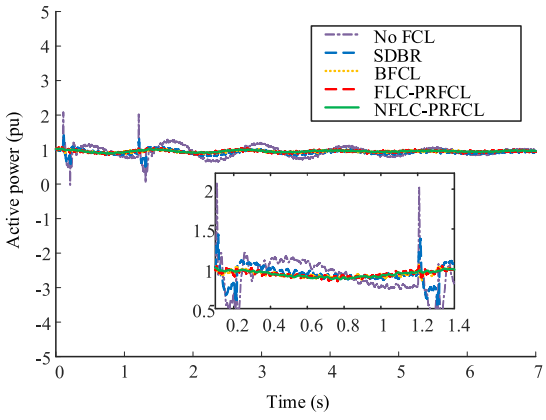

FIGURE 41. Active power response at the PCC for temporary 1LG fault.

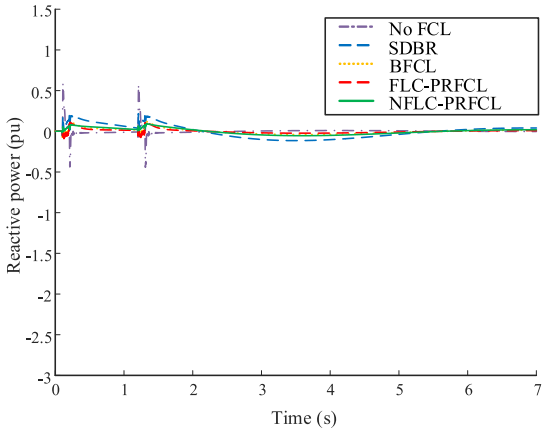

FIGURE 42. Reactive power at the PCC for permanent 1LG fault.

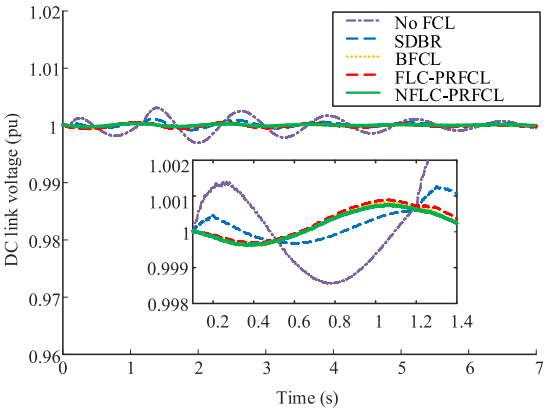

FIGURE 43. DC link voltage response for permanent 1LG fault.

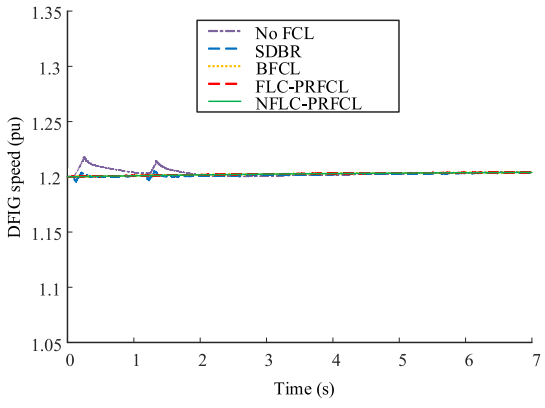

FIGURE 44. Speed response of the DFIG for permanent 1LG fault.

first sag as CBs open once again due to permanent faults before reaching the steady state condition. In Table 9 and Table 10, these responses are denoted by "N/A". Therefore, the settling time after the CBs open for the second time is also calculated for all the responses. It is evident that the proposed NFLC-PRFCL has the least settling time than the SDBR, BFCL, and FLC-PRFCL.

From the above analysis, it can be concluded that the proposed NFLC-PRFCL can enhance the FRT capability of DFIG based wind farms in a better way as compared to other three methods.

VII. DISCUSSION

The effectiveness of the proposed NFLC-PRFCL is evident from all the graphical and numerical analysis from the previous section. The graphical analysis of both temporary and permanent faults showed that the NFLC-PRFCL has been superior in keeping the system dynamics closer to normal during any abnormalities. The NFLC-PRFCL suppressed the

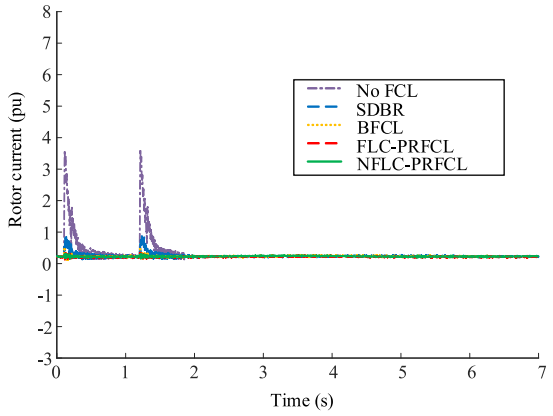

FIGURE 45. Rotor current for permanent 1LG fault.

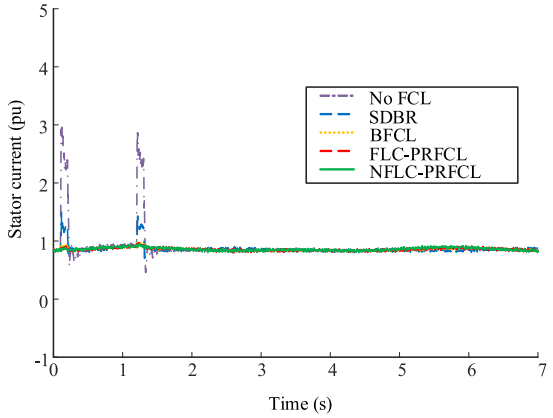

FIGURE 46. Stator current for permanent 1LG fault.

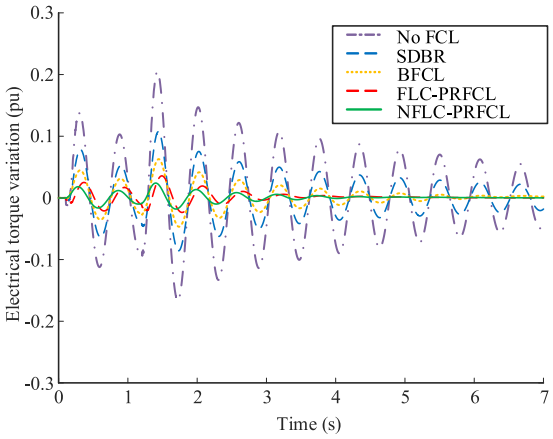

FIGURE 47. Electrical torque variations for permanent 1LG fault.

oscillations caused by system disturbances more efficiently than the FLC-PRFCL as well as the other FRT strategies. The index-based analysis demonstrated that the deviations of the responses with the presence of the NFLC-PRFCL occupies less area which resembles its better effectiveness. The NFLC-PRFCL also made sure the responses reach the steady state faster and has less amount of percentage overshoot

TABLE 7. Performance indices for permanent symmetrical (3LG) fault.

Index	Values of indices				
parameters (%)	No FCL	SDBR	BFCL	FLC-PRFCL	NFLC-PRFCL
vlt(pu.s)	20.266	3.413	2.491	1.189	0.801
pow(pu.s)	65.942	32.846	22.871	16.624	13.929
reactive(pu.s)	53.698	52.688	31.999	24.839	13.232
dclink(pu.s)	0.882	0.175	0.146	0.138	0.087
spd(pu.s)	14.675	4.437	3.148	2.663	2.132
rtr(pu.s)	108.096	23.375	15.094	5.102	5.003
str(pu.s)	55.758	42.689	23.925	12.268	11.089
torque(pu.s)	151.313	49.865	23.285	19.859	6.240

TABLE 8. Performance indices for permanent unsymmetrical (1LG) fault.

Index	Values of indices				
parameters (%)	No FCL	SDBR	BFCL	FLC-PRFCL	NFLC-PRFCL
vlt(pu.s)	7.955	2.534	1.296	0.584	0.441
pow(pu.s)	25.895	18.848	7.985	7.662	6.601
reactive(pu.s)	52.768	25.155	19.787	12.689	10.479
dclink(pu.s)	0.207	0.104	0.059	0.052	0.048
spd(pu.s)	10.848	3.489	1.486	1.442	1.286
rtr(pu.s)	75.949	15.895	7.386	3.211	3.025
str(pu.s)	38.848	20.846	8.488	7.332	6.529
torque(pu.s)	50.312	22.629	9.574	4.344	4.288

compared to other FRT strategies as shown in the steady state analysis for both temporary and permanent faults.

The NFLC-PRFCL incorporates self-adaptive learning algorithm that optimizes the value of membership functions of the FLC based on the variation of the system dynamics. In this work, the voltage deviation of the PCC, ΔV is sampled as the input of the FLC. Without the NFLC, the MF of the FLC is always constant regardless the change in system dynamics. This reduces the overall accuracy of the FLC-PRFCL. But, in case of NFLC-PRFCL, when there is any change in system dynamics due to variation in load or any reason, the NFLC-PRFCL can update the MF prior to the change. This eliminates the need of any manual control and makes the NFLC-PRFCL more efficient than the FLC-PRFCL and other traditional FCLs.

VIII. PRACTICALITY AND COST ANALYSIS

The total cost of the auxiliary FCLs depend on their relative rating and installation cost. The cost of the SDBR can be estimated from the 1400 MW Bonneville power administration (BPA) project. The project costed around $30-$40 million [54], [55]. The shunt connected switches of the braking resistor has a cost per unit MVA of $25-$30. The total cost covers the cost of installation and manufacturing. The exact cost of the BFCL cannot be estimated as it has no live grid industrial application yet. However, the BFCL consists of only diodes, resistors and inductors which can be easily implemented due to advancement in industrial power electronics and manufacturing industry. Similarly, the PRFCL has almost identical configuration to the BFCL except that it has an additional capacitor. Hence the cost of the BFCL and the PRFCL is equitable in comparison with the other proposed methodolo-

TABLE 9. Steady state analysis for permanent symmetrical (3LG) fault.

FCLs	Overshoot												Settling time											
	Active power		DC-link voltage		DFIG speed		Rotor current		Stator current		Torque		Active power		DC-link voltage		DFIG speed		Rotor current		Stator current		Torque	
	1st sag	2nd sag	1st sag	2nd sag	1st sag	2nd sag	1st sag	2nd sag	1st sag	2nd sag	1st sag	2nd sag	1st sag	2nd sag	1st sag	2nd sag	1st sag	2nd sag	1st sag	2nd sag	1st sag	2nd sag	1st sag	2nd sag
No FCL	49.693	46.460	0.099	0.299	2.201	1.534	94.592	94.607	79.059	77.400	96.790	97.634	N/A	14.146	N/A	∞	N/A	21.264	N/A	4.980	N/A	1.989	N/A	20.057
SDBR	48.571	42.857	0.065	0.082	1.381	1.397	77.619	76.766	56.699	56.410	86.729	90.440	0.649	0.827	N/A	2.747	N/A	6.267	0.622	0.808	N/A	0.988	N/A	17.047
BFCL	17.279	17.883	0.041	0.038	1.194	1.291	33.030	36.012	9.285	13.354	78.439	84.152	0.205	0.319	N/A	1.098	1.057	0.238	0.597	0.741	0.718	0.774	N/A	10.076
FLC-PRFCL	14.746	14.275	0.021	0.027	0.889	1.113	30.178	32.345	5.356	10.101	69.409	77.859	0.112	0.133	0.601	0.527	0.941	0.213	0.510	0.581	0.567	0.504	N/A	5.938
NFLC-PRFCL	12.467	12.124	0.011	0.014	0.221	0.493	20.128	27.364	3.156	6.339	47.257	62.714	0.080	0.104	0.556	0.498	0.528	0.201	0.483	0.492	0.494	0.375	N/A	3.136

TABLE 10. Steady state analysis for permanent unsymmetrical (1LG) fault.

FCLs	Overshoot												Settling time											
	Active power		DC-link voltage		DFIG speed		Rotor current		Stator current		Torque		Active power		DC-link voltage		DFIG speed		Rotor current		Stator current		Torque	
	1st sag	2nd sag	1st sag	2nd sag	1st sag	2nd sag	1st sag	2nd sag	1st sag	2nd sag	1st sag	2nd sag	1st sag	2nd sag	1st sag	2nd sag	1st sag	2nd sag	1st sag	2nd sag	1st sag	2nd sag	1st sag	2nd sag
No FCL	56.710	52.731	0.100	0.299	1.961	3.459	92.954	92.928	70.175	69.986	85.444	90.133	N/A	11.998	N/A	∞	N/A	19.247	N/A	4.906	N/A	1.906	N/A	14.077
SDBR	36.215	28.571	0.070	0.090	1.631	1.647	66.216	66.799	42.098	37.362	74.398	81.361	0.513	0.687	N/A	2.747	N/A	5.677	0.583	0.717	N/A	1.291	N/A	11.062
BFCL	17.582	18.404	0.020	0.040	0.753	0.835	45.887	46.467	9.188	14.055	55.267	68.168	0.474	0.196	N/A	1.118	0.129	0.212	0.425	0.614	0.548	0.649	N/A	7.174
FLC-PRFCL	13.464	15.363	0.012	0.023	0.528	0.483	35.376	43.283	4.736	8.365	20.096	43.993	0.338	0.140	0.762	0.894	0.137	0.166	0.299	0.514	0.441	0.519	N/A	3.28
NFLC-PRFCL	10.363	12.287	0.008	0.016	0.237	0.339	31.236	32.344	2.454	4.473	16.283	36.869	0.143	0.076	0.528	0.609	0.095	0.103	0.294	0.485	0.344	0.482	N/A	2.88

*N/A = Not applicable as the CBs open again before the responses can reach steady state.

TABLE 11. Comparison among the fault ride through enhancement methods.

Criteria	NFLC-PRFCL	FLC-PRFCL	BFCL	SDBR
Construction	Consists of a bridge circuit with four diodes and a resonant circuit of an inductor and a capacitor. Easy to implement.	Similar to the NFLC-PRFCL	Has a simple bridge structure. A single BFCL consists of four diodes, an IGBT, an inductor and a resistor. Easy to implement.	Has the simplest construction consisting a resistor and an IGBT.
FRT capability enhancement	Most effective to improve the FRT capability of DFIG based wind farms.	Effective but not up to the mark as the NFLC-PRFCL.	Very capable alternative to the PRFCL, but still falls behind of the PRFCL to some extent.	Effective method but not as good as the BFCL or the PRFCL.
Ability to control active and reactive power	Can control both active and reactive power.	Can control both active and reactive power.	Can control only active power.	Can control only active power.
Cost	Comparatively costlier than the BFCL but quite comfortably commercially viable. Easily affordable.	Similar to the NFLC-PRFCL	Slightly cheaper than the PRFCL. Mass production is possible.	Cheaper than both the BFCL and the PRFCL.
Structure of control system	Incorporates adaptive neuro fuzzy logic based control scheme. Can adapt to the variation in system dynamics.	Incorporates fuzzy logic based control scheme. The membership functions are constant regardless the variation in system dynamics.	Typically based on comparison logic based controllers. Can be developed using fuzzy logic and neuro fuzzy logic based controller.	Has simple comparison logic based controller. Less efficient in capturing system dynamics.

gies in the literature, as they do not have any superconducting parts and do not require expensive cryogenic cooling medium like the superconductors. A comprehensive comparison of the considered FRT methods based on different criteria is given in Table 11.

IX. CONCLUSION

In this paper, a neuro fuzzy logic controlled parallel resonance type fault current limiter (NFLC-PRFCL) is proposed to augment the FRT capability of the grid connected DFIG based wind farm. The performance of this control technique is compared with the performances of existing fuzzy logic controlled parallel resonance type fault current limiter (FLC-PRFCL) and two of the other frequently used conventional FCLs, bridge type fault current limiter (BFCL) and series dynamic braking resistor (SDBR). The system response in absence of any auxiliary controller is also considered during the comparison. Observing the simulation results and the numerical comparisons, the following conclusions can be reached:

- Without any FCL, the system experiences substandard consequences during fault. The FCLs offer a significant degree of improvement in the system responses.
- Compared to other traditional FCLs, the NFLC-PRFCL offers better responses.
- In terms of numerical indices, the NFLC-PRFCL presents better superiority over other FCLs considered in this work. For instance, the NFLC-PRFCL assured 97.10% of improvement of the PCC voltage during a temporary 3LG fault, while the SDBR, the BFCL and the FLC-PRFCL scored 84.09%, 87.77% and 94.45%, respectively.
- Also, during permanent fault due to unsuccessful reclosure of the CBs, the response of the NFLC-PRFCL

stands out as it provides 12.89%, 8.34% and 1.92% more improvement of PCC voltage than that of the SDBR, the BFCL and the FLC-PRFCL respectively.
- Additionally, the proposed NFLC-PRFCL is more efficient and effective due to its ability to adapt with the system dynamics variations.

In our future work, a prototype of the NFLC-PRFCL will be made to test the authenticity of this proposed control scheme practically. Furthermore, the NFLC-PRFCL is intended to be used in other grid connected renewable energy systems i.e. solar PV system, ocean energy system etc. In addition to that, we will be looking for more robust nonlinear controller for the PRFCL.

APPENDIX

The parameters of the DFIG and the drive train are provided in the Table 12.

TABLE 12. Each DFIG and drive train data.

Parameter	Value
Rated power	1.5 MVA
Rated voltage	0.69 KV
DC-link nominal voltage	1.2 KV
DC-link capacitance value	12000 μF
Wind speed	14 $m.s^{-1}$
Frequency	60 Hz
Resistance of stator	0.005 pu
Magnetizing inductance	3.95279 pu
Leakage inductance of stator	0.09321 pu
Inertia	0.80
Leakage inductance of wound rotor	0.09955 pu
Wound rotor resistance	0.0055 pu
Friction factor	0.01

REFERENCES

[1] T. K. Roy and M. A. Mahmud, "Active power control of three-phase grid-connected solar PV systems using a robust nonlinear adaptive backstepping approach," *Sol. Energy*, vol. 153, pp. 64–76, Sep. 2017.
[2] M. R. Islam, M. M. Hasan, F. R. Badal, S. K. Das, and S. K. Ghosh, "A blended improved h5 topology with ILQG controller to augment the performance of microgrid system for grid-connected operations," *IEEE Access*, vol. 8, pp. 69639–69660, 2020.
[3] Y. M. Alsmadi, L. Xu, F. Blaabjerg, A. J. P. Ortega, A. Y. Abdelaziz, A. Wang, and Z. Albataineh, "Detailed investigation and performance improvement of the dynamic behavior of grid-connected DFIG-based wind turbines under LVRT conditions," *IEEE Trans. Ind. Appl.*, vol. 54, no. 5, pp. 4795–4812, Sep. 2018.
[4] M. N. I. Sarkar, L. G. Meegahapola, and M. Datta, "Reactive power management in renewable rich power grids: A review of grid-codes, renewable generators, support devices, control strategies and optimization algorithms," *IEEE Access*, vol. 6, pp. 41458–41489, 2018.
[5] S. Tohidi and M.-I. Behnam, "A comprehensive review of low voltage ride through of doubly fed induction wind generators," *Renew. Sustain. Energy Rev.*, vol. 57, pp. 412–419, May 2016.
[6] J. J. Justo, F. Mwasilu, and J.-W. Jung, "Doubly-fed induction generator based wind turbines: A comprehensive review of fault ride-through strategies," *Renew. Sustain. Energy Rev.*, vol. 45, pp. 447–467, May 2015.
[7] M. R. Islam, M. N. Huda, M. M. Hasan, J. Hasan, and D. D. Abir, "Fault ride through capability enhancement of DFIG based wind farm using advanced converter topology," in *Proc. Int. Conf. Comput., Commun., Chem., Mater. Electron. Eng. (ICME)*, Jul. 2019, pp. 1–4.
[8] Z.-X. Zheng, C.-J. Huang, R.-H. Yang, X.-Y. Xiao, and C.-S. Li, "A low voltage ride through scheme for DFIG-based wind farm with SFCL and RSC control," *IEEE Trans. Appl. Supercond.*, vol. 29, no. 2, pp. 1–5, Mar. 2019.
[9] D. Xiang, L. Ran, P. J. Tavner, and S. Yang, "Control of a doubly fed induction generator in a wind turbine during grid fault ride-through," *IEEE Trans. Energy Convers.*, vol. 21, no. 3, pp. 652–662, Sep. 2006.
[10] M. K. Döşoğlu, U. Güvenç, Y. Sönmez, and C. Yılmaz, "Enhancement of demagnetization control for low-voltage ride-through capability in DFIG-based wind farm," *Elect. Eng.*, vol. 100, no. 2, pp. 491–498, Jun. 2018.
[11] D. Zhu, X. Zou, L. Deng, Q. Huang, S. Zhou, and Y. Kang, "Inductance-emulating control for DFIG-based wind turbine to ride-through grid faults," *IEEE Trans. Power Electron.*, vol. 32, no. 11, pp. 8514–8525, Nov. 2017.
[12] S. Xiao, G. Yang, H. Zhou, and H. Geng, "An LVRT control strategy based on flux linkage tracking for DFIG-based WECS," *IEEE Trans. Ind. Electron.*, vol. 60, no. 7, pp. 2820–2832, Jul. 2013.
[13] M. K. Döşoğlu, "Hybrid low voltage ride through enhancement for transient stability capability in wind farms," *Int. J. Elect. Power Energy Syst.*, vol. 78, pp. 655–662, Jun. 2016.
[14] C. Wessels, F. Gebhardt, and F. W. Fuchs, "Fault ride-through of a DFIG wind turbine using a dynamic voltage restorer during symmetrical and asymmetrical grid faults," *IEEE Trans. Power Electron.*, vol. 26, no. 3, pp. 807–815, Mar. 2011.
[15] W. Qiao, G. K. Venayagamoorthy, and R. G. Harley, "Real-time implementation of a STATCOM on a wind farm equipped with doubly fed induction generators," *IEEE Trans. Ind. Appl.*, vol. 45, no. 1, pp. 98–107, Jan. 2009.
[16] J. Liu, W. Yao, J. Fang, J. Wen, and S. Cheng, "Stability analysis and energy storage-based solution of wind farm during low voltage ride through," *Int. J. Elect. Power Energy Syst.*, vol. 101, pp. 75–84, Oct. 2018.
[17] S. M. Muyeen, R. Takahashi, T. Murata, J. Tamura, M. H. Ali, Y. Matsumura, A. Kuwayama, and T. Matsumoto, "Low voltage ride through capability enhancement of wind turbine generator system during network disturbance," *IET Renew. Power Gener.*, vol. 3, no. 1, pp. 65–74, Mar. 2009.
[18] M. R. Islam, M. G. Ajom, and M. R. I. Sheikh, "Application of DC chopper to augment fault ride through of DFIG based wind turbine," in *Proc. 2nd Int. Conf. Electr. Electron. Eng. (ICEEE)*, Dec. 2017, pp. 1–4.
[19] M. K. Döşoğlu, "Enhancement of SDRU and RCC for low voltage ride through capability in DFIG based wind farm," *Elect. Eng.*, vol. 99, no. 2, pp. 673–683, Jun. 2017.
[20] M. K. Döşoğlu, "A new approach for low voltage ride through capability in DFIG based wind farm," *Int. J. Elect. Power Energy Syst.*, vol. 83, pp. 251–258, Dec. 2016.
[21] M. Mahdianpoor, A. Kiyoumarsi, M. Ataei, and R.-A. Hooshmand, "Robust implementation of distribution static compensator along with bridge type fault current limiter for fault ride through enhancement of fixed speed wind turbines," *IEEE Access*, vol. 5, pp. 14490–14501, 2017.
[22] H.-T. Tseng, W.-Z. Jiang, and J.-S. Lai, "A modified bridge switch-type flux-coupling nonsuperconducting fault current limiter for suppression of fault transients," *IEEE Trans. Power Del.*, vol. 33, no. 6, pp. 2624–2633, Dec. 2018.
[23] Q. Yang, S. L. Blond, F. Liang, W. Yuan, M. Zhang, and J. Li, "Design and application of superconducting fault current limiter in a multiterminal HVDC system," *IEEE Trans. Appl. Supercond.*, vol. 27, no. 4, pp. 1–5, Jun. 2017.
[24] L. Qu, R. Zeng, Z. Yu, and G. Li, "Design and test of a magnetic saturation-type fault current limiter," *J. Eng.*, vol. 2019, no. 16, pp. 2974–2979, Mar. 2019.
[25] S. B. Naderi, M. Jafari, and M. Tarafdar Hagh, "Parallel-resonance-type fault current limiter," *IEEE Trans. Ind. Electron.*, vol. 60, no. 7, pp. 2538–2546, Jul. 2013.
[26] M. E. Elshiekh, D.-E. A. Mansour, and A. M. Azmy, "Improving fault ride-through capability of DFIG-based wind turbine using superconducting fault current limiter," *IEEE Trans. Appl. Supercond.*, vol. 23, no. 3, Jun. 2012, Art. no. 5601204.
[27] Z.-C. Zou, X.-Y. Xiao, Y.-F. Liu, Y. Zhang, and Y.-H. Wang, "Integrated protection of DFIG-based wind turbine with a resistive-type SFCL under symmetrical and asymmetrical faults," *IEEE Trans. Appl. Supercond.*, vol. 26, no. 7, pp. 1–5, Oct. 2016.
[28] Z.-C. Zou, X.-Y. Chen, C.-S. Li, X.-Y. Xiao, and Y. Zhang, "Conceptual design and evaluation of a resistive-type SFCL for efficient fault ride through in a DFIG," *IEEE Trans. Appl. Supercond.*, vol. 26, no. 1, pp. 1–9, Jan. 2016.

[29] H.-J. Lee, S.-H. Lim, and J.-C. Kim, "Application of a superconducting fault current limiter to enhance the low-voltage ride-through capability of wind turbine generators," *Energies*, vol. 12, no. 8, p. 1478, Apr. 2019.

[30] M. R. Islam, D. D. Abir, M. R. Islam, J. Hasan, M. N. Huda, K. M. Muttaqi, and D. Sutanto, "Enhancement of FRT capability of DFIG based wind farm by a hybrid superconducting fault current limiter with bias magnetic field," in *Proc. IEEE Int. Conf. Power Electron., Smart Grid Renew. Energy (PESGRE)*, Jan. 2020, pp. 1–6.

[31] J. Yuan, Y. Zhong, Y. Lei, C. Tian, W. Guan, Y. Gao, K. Muramatsu, and B. Chen, "A novel hybrid saturated core fault current limiter topology considering permanent magnet stability and performance," *IEEE Trans. Magn.*, vol. 53, no. 6, pp. 1–4, Jun. 2017.

[32] A. Causebrook, D. J. Atkinson, and A. G. Jack, "Fault ride-through of large wind farms using series dynamic braking resistors (March 2007)," *IEEE Trans. Power Syst.*, vol. 22, no. 3, pp. 966–975, Aug. 2007.

[33] G. Rashid and M. Hasan Ali, "A modified bridge-type fault current limiter for fault ride-through capacity enhancement of fixed speed wind generator," *IEEE Trans. Energy Convers.*, vol. 29, no. 2, pp. 527–534, Jun. 2014.

[34] G. Rashid and M. H. Ali, "Transient stability enhancement of doubly fed induction machine-based wind generator by bridge-type fault current limiter," *IEEE Trans. Energy Convers.*, vol. 30, no. 3, pp. 939–947, Sep. 2015.

[35] G. Rashid and M. H. Ali, "Application of parallel resonance fault current limiter for fault ride through capability augmentation of DFIG based wind farm," in *Proc. IEEE/PES Transmiss. Distrib. Conf. Expo. (T&D)*, May 2016, pp. 1–5.

[36] M. A. H. Sadi and M. H. Ali, "Transient stability enhancement of multimachine power system by parallel resonance type fault current limiter," in *Proc. North Amer. Power Symp. (NAPS)*, Oct. 2015, pp. 1–6.

[37] M. R. Islam, M. N. Huda, J. Hasan, M. A. H. Sadi, A. AbuHussein, T. K. Roy, and M. A. Mahmud, "Fault ride through capability improvement of DFIG based wind farm using nonlinear controller based bridge-type flux coupling non-superconducting fault current limiter," *Energies*, vol. 13, no. 7, p. 1696, Apr. 2020.

[38] R. A. J. Amalorpavaraj, P. Kaliannan, S. Padmanaban, U. Subramaniam, and V. K. Ramachandaramurthy, "Improved fault ride through capability in DFIG based wind turbines using dynamic voltage restorer with combined feed-forward and feed-back control," *IEEE Access*, vol. 5, pp. 20494–20503, 2017.

[39] G. Rashid and M. H. Ali, "Fault ride through capability improvement of DFIG based wind farm by fuzzy logic controlled parallel resonance fault current limiter," *Electr. Power Syst. Res.*, vol. 146, pp. 1–8, May 2017.

[40] M. R. Islam and M. R. I. Sheikh, "Transient stability enhancement of DFIG based wind generator by switching frequency control strategy with parallel resonance fault current limiter," *Global J. Researches Eng., Elect. Electron. Eng.*, vol. 18, no. 1, pp. 39–48, Mar. 2018.

[41] M. K. Hossain and M. H. Ali, "Transient stability augmentation of PV/DFIG/SG-based hybrid power system by parallel-resonance bridge fault current limiter," *Electr. Power Syst. Res.*, vol. 130, pp. 89–102, Jan. 2016.

[42] M. K. Hossain and M. H. Ali, "Transient stability augmentation of PV/DFIG/SG-based hybrid power system by nonlinear control-based variable resistive FCL," *IEEE Trans. Sustain. Energy*, vol. 6, no. 4, pp. 1638–1649, Oct. 2015.

[43] D.-N. Truong and V.-T. Ngo, "Designed damping controller for SSSC to improve stability of a hybrid offshore wind farms considering time delay," *Int. J. Electr. Power Energy Syst.*, vol. 65, pp. 425–431, Feb. 2015.

[44] M. A. H. Sadi and M. H. Ali, "A fuzzy logic controlled bridge type fault current limiter for transient stability augmentation of multi-machine power system," *IEEE Trans. Power Syst.*, vol. 31, no. 1, pp. 602–611, Jan. 2016.

[45] A. Benali, M. Khiat, T. Allaoui, and M. Denai, "Power quality improvement and low voltage ride through capability in hybrid wind-PV farms grid-connected using dynamic voltage restorer," *IEEE Access*, vol. 6, pp. 68634–68648, 2018.

[46] M. R. Islam, J. Hasan, M. N. Huda, and M. A. H. Sadi, "Fault ride through capability improvement of DFIG based wind farms using active power controlled bridge type fault current limiter," in *Proc. North Amer. Power Symp. (NAPS)*, Oct. 2019, pp. 1–6.

[47] K. E. Okedu, S. M. Muyeen, R. Takahashi, and J. Tamura, "Wind farms fault ride through using DFIG with new protection scheme," *IEEE Trans. Sustain. Energy*, vol. 3, no. 2, pp. 242–254, Apr. 2012.

[48] J. López, P. Sanchis, X. Roboam, and L. Marroyo, "Dynamic behavior of the doubly fed induction generator during three-phase voltage dips," *IEEE Trans. Energy Convers.*, vol. 22, no. 3, pp. 709–717, Sep. 2007.

[49] G. Rashid and M. H. Ali, "Nonlinear control-based modified BFCL for LVRT capacity enhancement of DFIG-based wind farm," *IEEE Trans. Energy Convers.*, vol. 32, no. 1, pp. 284–295, Mar. 2017.

[50] General Atomics Electromagnetic Systems. (2020). *High Voltage Capacitors and Power Supplies*. [Online]. Available: http://www.ga.com/capacitors

[51] J.-S.-R. Jang, "ANFIS: Adaptive-network-based fuzzy inference system," *IEEE Trans. Syst., Man, Cybern.*, vol. 23, no. 3, pp. 665–685, May 1993.

[52] S. R. Khuntia and S. Panda, "ANFIS approach for SSSC controller design for the improvement of transient stability performance," *Math. Comput. Model.*, vol. 57, nos. 1–2, pp. 289–300, Jan. 2013.

[53] M. H. Ali, M. Park, I.-K. Yu, T. Murata, J. Tamura, and B. Wu, "Enhancement of transient stability by fuzzy logic-controlled SMES considering communication delay," *Int. J. Elect. Power Energy Syst.*, vol. 31, nos. 7–8, pp. 402–408, Sep. 2009.

[54] M. L. Shelton, P. F. Winkelman, W. A. Mittelstadt, and W. J. Bellerby, "Bonneville power administration 1400-MW braking resistor," *IEEE Trans. Power App. Syst.*, vol. PAS-94, no. 2, pp. 602–611, Mar. 1975.

[55] M. A. H. Sadi and M. H. Ali, "A comprehensive analysis of transient stability enhancement methods of electric power system," in *Proc. North Amer. Power Symp. (NAPS)*, Oct. 2015, pp. 1–6.

MD. RASHIDUL ISLAM received the B.Sc. and M.Sc. degrees in electrical and electronic engineering (EEE) from the Rajshahi University of Engineering and Technology (RUET), Rajshahi, Bangladesh, in 2013 and 2017, respectively.

He was a Lecturer with the Department of EEE, Varendra University, Rajshahi. He is currently working as an Assistant Professor with the Department of EEE, RUET. His research interests include nonlinear controller design and applications on renewable energy systems, the applications of power electronics in renewable energy, microgrid systems, and fault ride through capability augmentation. He received the University Gold Medal Award from the RUET. He also received the Prime Minister Gold Medal Award.

JAKIR HASAN was born in Natore, Bangladesh, in 1996. He received the B.Sc. degree in electrical and electronic engineering (EEE) from the Rajshahi University of Engineering and Technology, in 2019. His research interests include renewable energy systems, microgrids, ride through capability augmentation, and nonlinear controller design and its applications.

MD. REZAUR RAHMAN SHIPON was born in Kurigram, Bangladesh, in 1998. He is currently pursuing the bachelor's degree in electrical and electronic engineering (EEE) with the Rajshahi University of Engineering and Technology (RUET), Rajshahi, Bangladesh. His current research interests include smart grids and microgrid systems, power electronics, renewable energy systems, and power system control.

MOHAMMAD ASHRAF HOSSAIN SADI (Senior Member, IEEE) received the Ph.D. degree in electrical engineering from the University of Memphis, in 2016. He is currently an Assistant Professor with the University of Central Missouri, Warrensburg, USA. His main fields of interest include advanced power systems, smart-grid and micro-grid systems, renewable energy systems, and flexible ac transmission systems (FACTS). He is also a member of the IEEE Power and Energy Society.

AHMED ABUHUSSEIN (Member, IEEE) is currently an Assistant Professor in the Department of electrical and computer engineering (ECE) at Gannon University. He received his Ph.D. degree in ECE from the University of Memphis, Tennessee, USA. He also holds a MS degree in ECE from the same institute and a BS degree in electrical power engineering from Tafila Technical University (TTU), Tafila, Jordan. His main field of interest includes fault current limiters, power quality, geomagnetically induced currents (GIC), power electronics, electrical machines, AC/DC microgrids, renewable energy systems, energy storage systems, and flexible AC transmission systems (FACTS).

TUSHAR KANTI ROY received the B.Sc. degree in electrical and electronic engineering (EEE) from the Rajshahi University of Engineering and Technology, Rajshahi, Bangladesh, in 2008, the M.Eng. (research) degree in electrical engineering from the University of New South Wales, Canberra, ACT, Australia, in 2012, and the Ph.D. degree in electrical engineering from Deakin University, Melbourne, Australia, in 2019.

He is currently working as an Assistant Professor with the Department of electronics and telecommunication engineering, Rajshahi University of Engineering and Technology, where he also worked as a Lecturer. His research interests include nonlinear control theory and its applications, excitation control, microgrids, renewable energy, and power electronics.